

Maria Bjelland

Biocorrosion Resistance of Mg alloy AZ31 Nanocoated with ZrO_2 , HfO_2 and TiO_2 by Atomic Layer Deposition Method

June 2019



Norwegian University of
Science and Technology

Biocorrosion Resistance of Mg alloy AZ31 Nanocoated with ZrO_2 , HfO_2 and TiO_2 by Atomic Layer Deposition Method

Maria Bjelland

Mechanical Engineering

Submission date: June 2019

Supervisor: Jan Torgersen

Co-supervisor: Mirco Peron

Norwegian University of Science and Technology
Department of Mechanical and Industrial Engineering

Preface

This master thesis is written during the spring semester of 2019. The thesis is submitted to the Norwegian University of Science and Technology (NTNU) in Trondheim, as a part of the study programme Mechanical Engineering. The report is carried out at the Department of Mechanical and Industrial Engineering (MTP), within the specialization field Product Development and Materials (PuMa), and is supervised by Associate Professor Jan Torgersen.

The work in this thesis is based on the literature study done in my specialization project "Surface coatings prepared by Atomic Layer Deposition to improve the biocorrosion resistance of magnesium alloys", written during the autumn semester of 2018.

I declare that this work has been performed independently and in accordance with the rules and regulations at NTNU.

Maria Bjelland
Trondheim, 2019-06-11

Abstract

Due to magnesium alloys excellent bio-compatibility with human physiology, and the great mechanical compatibility with human bone, they are considered suitable for biomedical implant devices. However, their rapid corrosion rate in the human body environment limits their use in clinical applications. Recently, a coating technique called Atomic Layer Deposition (ALD) has gained attention for biocorrosion protection of magnesium as it offers very thin, conformal and pin-hole free coatings.

In this master thesis, ZrO_2 -, HfO_2 -, and TiO_2 -coatings prepared by ALD were deposited on magnesium alloy AZ31 to assess ALD's applicability as a method to reduce the corrosion rate of this alloy. The coatings performances were evaluated through potentiodynamic polarisation tests, electrochemical impedance spectroscopy, and hydrogen evolution measurements. The results showed that all the different ALD-coatings improved the corrosion resistance of the alloy. However, the corrosion rate of the ALD-coated AZ31-samples is still too high to allow the use in biomedical applications, and further research is necessary.

Sammendrag

Magnesiumlegeringer med sin utmerkede kombinasjon av mekaniske egenskaper og biokompatibilitet, gjør dem egnet for biomedisinske implantater. Imidlertid begrenser deres høye korrosjonsrate i menneskekroppsmiljøet deres bruk i kliniske applikasjoner. Nylig har en coatemetode kalt «Atomic Layer Deposition» (ALD), fått oppmerksomhet for biokorrosjonsbeskyttelse av magnesium, fordi den gir svært tynne, presise og tette coatinger.

I denne masteroppgaven ble ZrO_2 -, HfO_2 - og TiO_2 -coatinger ved hjelp av ALD påført magnesiumlegering AZ31 for å undersøke om ALD er en egnet metode for å forbedre korrosjonsresistansen til legeringen. Egenskapene til coatingene ble evaluert gjennom potensiodynamiske polarisasjonstester, elektrokjemisk impedansspektroskopi og hydrogenutviklingsmålinger. Resultatene viste at alle ALD-coatingene forbedret magnesiumlegeringens korrosjonsmotstand. Imidlertid var korrosjonshastigheten til AZ31-prøvene fortsatt for høy til bruk i biomedisinske applikasjoner, og videre testing er nødvendig.

Acknowledgment

I would like to express my gratitude to my supervisor, Associate Professor Jan Torgersen, and co-supervisor Ph.D. candidate Mirco Peron, for excellent guidance and help whenever I have needed it throughout the semester.

I would also like to thank Ph.D. candidate Abdulla Shaikh Abdul Qader Bin Affif for all the help and time spent with Atomic Layer Deposition, and Spectroscopic Ellipsometry.

A special thanks also goes to Ph.D. candidate Ellen Synnøve Skilbred and Ph.D. candidate Christian Torres Rodriguez for helping me in the corrosion laboratory at NTNU/SINTEF.

Lastly, the Research Council of Norway is acknowledged for the support to the Norwegian Micro- and Nano-Fabrication Facility, NorFab.

Contents

Preface	i
Abstract	iii
Sammendrag	v
Acknowledgement	vii
List of Figures	xii
List of Tables	xiv
Abbreviations	xv
1 Introduction	1
1.1 Background	1
1.2 Objectives	4
1.3 Scope	4
2 Theory	5
2.1 Corrosion of magnesium	5
2.1.1 Corrosion mechanism	5
2.1.2 Different types of corrosion	7
2.1.3 Corrosion challenges	10
2.1.4 Overcoming challenges	11
2.2 Atomic layer deposition	13

2.2.1	An introduction to the ALD-process	13
2.2.2	ALD compared to other coating techniques	14
2.2.3	Magnesium and ALD	16
2.2.4	Biocompatible thin-films	17
2.3	Principles behind the experimental methods	18
2.3.1	Potentiodynamic polarisation tests	18
2.3.2	Electrochemical Impedance Spectroscopy	21
2.3.3	Hydrogen evolution	23
3	Experimental Procedure	25
3.1	Materials	25
3.2	Sample preparation	25
3.3	Atomic layer deposition	25
3.4	Scanning Electron Microscopy	26
3.5	Electrolyte	26
3.6	Test set-ups	27
3.6.1	Potentiodynamic polarization curves	27
3.6.2	Electrochemical Impedance Spectroscopy	28
3.6.3	Hydrogen evolution	28
4	Results	29
4.1	Surface characterization	29
4.2	Potentiodynamic polarization curves	30

4.3	Electrochemical impedance spectroscopy	33
4.4	Hydrogen evolution	36
5	Discussion	37
5.1	Corrosion mechanism of the ALD-coated magnesium alloy AZ31 . . .	37
5.2	Comparison of coating performance on AZ31	38
5.3	Coating thickness	39
5.4	Biocompatibility of ALD-coatings	39
5.5	Suggestions for improving corrosion performance of ALD-coatings . .	40
5.6	Evaluation of experimental work	40
6	Conclusion	41
	References	42
	Appendices	I
A	Specialization project	I
B	Potentiodynamic polarisation curves	XLIII
C	Risk assessment	XLV

List of Figures

2.1	Galvanic corrosion between a gold fixation scrw and a magnesium implant, revised from [1]. The gold fixation screw drives electrons from the magnesium implant due to their potential difference, causing corrosion.	8
2.2	Galvanic corrosion between magnesium and second phases/impurities elements, revised from [1]. The cathodic elements drives electrons from the Mg matrix, causing dissolution of the magnesium.	9
2.3	Pitting corrosion starting on the magnesium surface, revised from [1]. The dissolution of magnesium inside the pit attracts Cl-ions to neutralise the charge, causing an aggressive corrosive environment inside the pit.	10
2.4	Illustration of the four steps in the atomic layer deposition process [2].	13
2.5	Evan’s diagram for a metal (Me), revised from [3].	20
2.6	The dotted lines shows the theoretical Tafel lines and the solid lines shows the experimental polarisation curves (For an active metal (Me) in an oxygen-free acidic solution). Revised from [3].	21
3.1	Set-up for the potentiodynamic polarisation tests.	27
3.2	Schematic illustration of the hydrogen evolution experiment.	28
4.1	SEM-pictures of different AZ31-samples where (a) Untreated (b) Coated with ZrO ₂ (c) Coated with HfO ₂ (d) Coated with TiO ₂	29
4.2	Potentiodynamic polarisation curves for coated and bare samples in SBF.	30
4.3	Potentiodynamic polarisation curves for coated and bare samples in SBF, close up of Figure 4.2.	30
4.4	Samples after potentiodynamic polarisation testing where (a) Bare (b) Coated with ZrO ₂ (c) Coated with HfO ₂ and (d) Coated with TiO ₂	31

4.5	SEM-images of samples after potentiodynamic polarisation tests, where (a) Bare (b) Magnification of a (c) ZrO ₂ -coated (d) Magnification of c (e) HfO ₂ -coated (f) Magnification of e (g) TiO ₂ -coated (h) Magnification of g.	32
4.6	Nyquist plots for the different samples a) Bare b) Coated with ZrO ₂ c) Coated with HfO ₂ d) Coated with TiO ₂	33
4.7	Bode plots for the different samples a) Bare b) Coated with ZrO ₂ c) Coated with HfO ₂ d) Coated with TiO ₂	34
4.8	Equivalent circuit for EIS.	35
4.9	Hydrogen evolution of different AZ31 samples.	36
B.1	The potentiodynamic polarisation curves for the bare samples. Note that the first sample was conducted with an electrode potential from -1 to 1 V relative to the OCP.	XLIII
B.2	The potentiodynamic polarisation curves for the ZrO ₂ -coated samples.	XLIII
B.3	The potentiodynamic polarisation curves for the HfO ₂ -coated samples.	XLIV
B.4	The potentiodynamic polarisation curves for the TiO ₂ -coated samples.	XLIV

List of Tables

1	Mechanical properties of natural bone and different implant materials [4].	2
2	The standard electromotive force series (EMF-series). The series rank metals based on their reactivity, where the metals on top are most reactive, and the metals in the bottom are least reactive. [5] .	5
3	Results from polarization tests conducted on coatings prepared by ALD.	16
4	Thickness and number of cycles for the different coatings.	26
5	The ion-concentration of SBF compared to blood plasma.	26
6	Corrosion potential and corrosion current density of the bare and coated samples.	31
7	Fitting results for EIS.	35

Abbreviations

ALD	Atomic Layer Deposition
CVD	Chemical Vapor Deposition
CPE	Constant Phase Element
EIS	Electrochemical Impedance Spectroscopy
EMF	Electromotive Force
OCP	Open Circuit Potential
PEO	Plasma Electrolytic Oxidation
PVD	Physical Vapor Deposition
SEM	Scanning Electron Microscopy
SBF	Simulated Body Fluid

1 Introduction

1.1 Background

Over the last decades, biomedical implants have had a vital role in improving the life quality of the world's population. The applications of implants are, amongst others, orthopaedics, cardiovascular stents, and neural prosthesis where the aim is to either replace or repair diseased parts of the human body. Of the various applications, orthopaedic surgery stands out having the highest annual growth rate [6]. According to Long and Rach [7], more than 90% of people above 40 years suffers of degenerative hip joint disease. For such fractures, surgical implantation of biomedical devices is an effective way to restore the load-bearing capacity of the damaged bone tissue.

Biomedical implants can be classified as either permanent or temporary. Permanent implants are required when lifetime support is necessary, as for instance with joint replacements. Depending on their area of application, several materials are suited for being permanent implants; various polymers, metals, ceramics, and composite materials [4]. However, due to their excellent mechanical properties, such as strength, toughness, and long service life, metals out-perform the other materials in the case of load-bearing applications. Due to the limitations of biocompatibility, the most commonly used metals are titanium and titanium alloys, stainless steels, and cobalt-chrome alloys [8, 9]. Moreover, there are several limitations to these metallic implants.

Firstly, the mechanical properties of the current implants highly differ from the mechanical properties of natural bone, as shown in Table 1. Such a mismatch leads to the stress shielding phenomenon. With stress shielding, the implant carries more load than the bone, and the bone adapts to this change, thus changing its properties [10]. The bone can either become thinner or more porous, both enhancing the risk of implant failure [4]. Secondly, in the long term, toxic ions or particles can be released from the implant due to corrosion and wear processes [9], and cause inflammations. Due to these causes, the maximum service time of an implant is about 12-15 years [11]. Hence, a patient will need a second surgery to remove the implant after healing. These surgeries can be complicated, and will expose the patient to the risk that comes with all surgeries.

Properties	Natural bone	Stainless Steel	Ti Alloy	Co-Cr Alloy	Magnesium
Density (g/cm ³)	1.7-2.0	7.9-8.1	4.4-4.5	8.3-9.2	1.74-2.0
Elastic modulus (MPa)	3-20	189-205	110-117	230	41-45
Tensile strength (MPa)	80-150	480-620	930-1140	900-1540	170-270
Compressive yield strength (MPa)	130-180	170-310	758-1117	450-1000	65-100
Elongation at failure (%)	1-7	30-40	8-15	30-45	6-20
Fracture toughness (MPa m ^{1/2})	3-6	50-200	55-115	100	15-40

Table 1: Mechanical properties of natural bone and different implant materials [4].

Opposed to permanent implants, temporary devices are only required to stay in the body for a limited time. This time is usually until the bone has healed, which is about 3-4 months [12]. Therefore biodegradable materials are now widely studied for scaffolds, and applications such as stents and bone fixators (screws, bone plates, and pins), where the implant device can degrade while the diseased tissue heals. Thus, they can overcome the challenges that come with permanent implants. Being biodegradable, a material can corrode inside the body with biocompatible degradation products [13]. In the last years, different biodegradable materials have been studied. Polymers have for example successfully been used for tissue engineering [14, 15, 16] and biodegradable sutures, drug delivery systems, fixations screws, and low load-bearing applications [17, 18, 19]. However, due to their limited mechanical properties, polymers do not guarantee sufficient mechanical performance for load-bearing applications. Additionally, they may absorb liquids and swell, leach undesirable products, and their performance can be affected by the sterilization process [20]. Therefore, the spotlight has been moved to biodegradable metal alloys, which provide sufficient mechanical properties and biocompatibility.

Amongst the biodegradable metal alloys available, involving iron-based metals, zinc-based metals, and tungsten [21], magnesium and its alloys have been widely studied due to their excellent biocompatibility [22]. With mechanical properties very similar to natural bone, as gathered in Table 1, the stress shielding phenomena is reduced [8]. As magnesium can degrade naturally within the body, the need for second surgeries and hence complications that comes with post-surgeries are removed [9]. Magnesium is also a vital part of the metabolism in the human body, crucial for many enzymes, and helps to stabilize DNA and RNA [23]. It is naturally found in the bone tissue, and magnesium cations are the fourth most abundant cations in the human body, where around 35 g magnesium per 70 kg body weight is usually contained in the human body [9]. A daily intake of 240-420

mg is also recommended for an adult [24]. On the other hand, too high levels of magnesium can give critical consequences, but this is rare as the body efficiently excretes excess magnesium in the urine [23].

The biggest challenge that comes with magnesium in biodegradable implants, is the poor corrosion resistance of the material. Magnesium's rapid corrosion rate will cause magnesium implants to suffer from early loss of mechanical properties, which furthermore can lead to implant failure before the surrounding tissue has time to heal [25]. Additionally, during the corrosion process of magnesium hydrogen gas will evolve, as will be described later in Section 2.1. When the rate of hydrogen evolution is too high, the human body will not be able to absorb all the gas. Hydrogen gas bubbles can therefore potentially go into the blood veins and block the bloodstream of a patient [4]. It has also been reported that hydrogen can cause necrosis in the area around the implant [26].

To utilize the potential of magnesium as biodegradable implants, the corrosion resistance needs to be improved. There are mainly two ways to improve the corrosion protection properties of magnesium; alloying, and coating. With alloying one can optimize the composition, microstructure and surface morphology [27], which can increase the degradation resistance. However, due to many alloying elements having a low solid solubility limit in magnesium, the obtained corrosion resistance by alloying alone is limited [28]. With a coating on the other hand, one can prevent fluid from entering the magnesium substrate and hence hinder corrosion. Therefore, applying coatings is an effective way of delaying the initial corrosion of magnesium alloys.

For biomedical applications, there are several requirements for a surface coating. Most importantly, the coating must be non-toxic, thus not cause any harm to the surrounding environment [25]. As the surface of the implant is where cells and new tissue will form, the coating must be biocompatible for these to adhere and grow. This is in regards to both surface morphology and coating composition. Additionally, as magnesium is biodegradable, so must the coating be. To be able to control and predict the degradation rate, uniform corrosion is desired, and it is therefore also advantageous if the coating has a uniform thickness. Being uniform, this also involve being pore free. Although pores may induce osseointegration [29], the path for fluids to reach the surface are reduced when pores are present. Moreover, pores enhance the possibility of localized corrosion which further can introduce the corrosion induced cracking phenomenon [4].

1.2 Objectives

Recently, a coating technique called Atomic layer deposition (ALD) has gained attention for corrosion protection as it offers very thin, precise, conformal and pin-hole free coatings. The ALD process allows to build coatings layer by layer, and to control the thickness on atom-scale. However, so far, little has been published regarding ALD's ability to improve the corrosion resistance of magnesium alloys for biomedical purposes.

The aim of this master thesis is therefore to investigate the protective properties of ALD-coatings on magnesium alloy AZ31. Additionally, the suitability of this coating technique to improve the corrosion resistance-, and delaying the degradation of alloy AZ31 for biomedical purposes, will be assessed.

1.3 Scope

In the reach of improving the corrosion performance of magnesium alloy AZ31, the effect of different coating materials prepared by ALD were evaluated. The different coating materials tested were Zirconia (ZrO_2), Hafnia (HfO_2) and Titania (TiO_2), which all are well-known ALD-materials. Zirconia was chosen because of its brilliant chemical stability and resistance to wear [30], and additionally has been shown to favour osseointegration and cytocompatibility [31]. Titania was chosen because it has good chemical and physical stability [32], is non-toxic for the human body, and has anti-bacterial properties [33]. Both Zirconia and Titania prepared by ALD had previously been evaluated for corrosion protection of magnesium, while Hafnia had not. However, because Hafnium is in the same chemical group as Titanium and Zirconium, Hafnia was expected to have similar properties as the other two.

The coatings abilities to protect the magnesium substrate from corrosion were evaluated by potentiodynamic polarisation tests, electrochemical impedance spectroscopy (EIS), and hydrogen evolution measurements. All experiments were conducted in room temperature. The coated and corroded surfaces were examined by Scanning Electron Microscopy (SEM).

2 Theory

2.1 Corrosion of magnesium

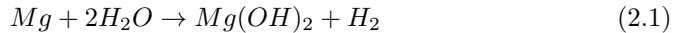
2.1.1 Corrosion mechanism

In a dry environment, magnesium and magnesium alloys will be stable and inert. In a humid environment or an aqueous solution, on the other hand, magnesium-based materials are prone to corrosion due to magnesium's highly negative electrode potential, as shown in the electromotive force series (EMF), also known as the electrochemical series, in Table 2. When corroding, free magnesium ions travel from the metal surface and to the adjacent aqueous environment. These free ions react with the environment and create compounds as for instance, hydroxides and metal oxides. These compounds will deposit on the metal surface and can, therefore, work as a physical barrier for corrosion depending on their solubility [1].

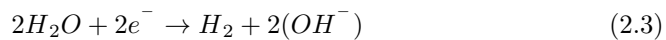
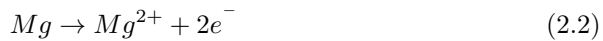
Table 2: The standard electromotive force series (EMF-series). The series rank metals based on their reactivity, where the metals on top are most reactive, and the metals in the bottom are least reactive. [5]

		Electrode	Electrode reaction	Standard Electrode Potential (V)
↑	Increasing active (Anodic)	Li, Li ⁺	$Li^+ + e^- \rightarrow Li$	-3.02
		K, K ⁺	$K^+ + e^- \rightarrow K$	-2.92
		Na, Na ⁺	$Na^+ + e^- \rightarrow Na$	-2.71
		Mg, Mg²⁺	$Mg^{2+} + 2e^- \rightarrow Mg$	-2.37
		Al, Al ³⁺	$Al^{3+} + 3e^- \rightarrow Al$	-1.66
		Zn, Zn ²⁺	$Zn^{2+} + 2e^- \rightarrow Zn$	-0.76
		Cr, Cr ³⁺	$Cr^{3+} + 3e^- \rightarrow Cr$	-0.74
		Fe, Fe ²⁺	$Fe^{2+} + 2e^- \rightarrow Fe$	-0.44
		Cd, Cd ²⁺	$Cd^{2+} + 2e^- \rightarrow Cd$	-0.40
		Co, Co ²⁺	$Co^{2+} + 2e^- \rightarrow Co$	-0.28
		Ni, Ni ²⁺	$Ni^{2+} + 2e^- \rightarrow Ni$	-0.25
		Sn, Sn ²⁺	$Sn^{2+} + 2e^- \rightarrow Sn$	-0.14
		Pb, Pb ²⁺	$Pb^{2+} + 2e^- \rightarrow Pb$	-0.13
		H₂, H⁺	$2H^+ + 2e^- \rightarrow H_2$	0.00
		Cu, Cu ²⁺	$Cu^{2+} + 2e^- \rightarrow Cu$	0.34
		Ag, Ag ⁺	$Ag^+ + e^- \rightarrow Ag$	0.80
		↓	Increasing inert (Cathodic)	Pt, Pt ²⁺
Au, Au ³⁺	$Au^{3+} + 3e^- \rightarrow Au$			1.42

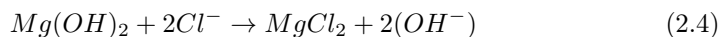
When magnesium is exposed to an aqueous environment, the metal will react with water, and a layer of magnesium hydroxide will form as according to Equation 2.1 [34].



The anodic and cathodic partial reactions are given in Equation 2.2 and 2.3 respectively.



The reaction in Equation 2.1 occurs randomly across the metal surface until the entire surface is covered. As magnesium hydroxide has low solubility in water, this layer has a protective function, and further corrosion of magnesium will be hindered. However, magnesium hydroxide is slightly soluble in water, and when chloride-ions are present, as is the case in human body fluid, the two species will react. The chloride-ions and magnesium hydroxide react and form magnesium chloride as according to equation 2.4 [34].



Unfortunately, magnesium chloride is highly soluble in water. As the chloride-ions will remove the protective hydroxide on the Mg-surface, solid magnesium will continue to react with water, and continue the corrosion process as in equation 2.1 [34].

It is important to be aware that if magnesium is to be used in a biodegradable implant, the degradation will be different in comparison to industrial applications as there are more factors affecting corrosion. These factors include, amongst others, the pH of the body fluid and variations of it, concentrations of ions, presence of proteins and level of protein adsorption on the implant and the impact from adjacent tissue [1].

2.1.2 Different types of corrosion

There are several different ways for magnesium and magnesium alloys to corrode. The biggest difference in the form of corrosion is whether the corrosion is uniform or localized. Uniform corrosion occurs evenly across a surface exposed in a corrosive environment, and is, thus, the most wanted corrosion mode as this ensures steady degradation [1]. Localized corrosion, on the other hand, takes place on local sites where the corrosion rate is more rapid than the rest of the surface. This form of corrosion is therefore hard to predict, can lead to toxicity and give sudden loss in mechanical performance [35]. However, in magnesium and magnesium alloys second phases, precipitates or impurities are always present. These are cathodic with respect to the magnesium matrix, and hence magnesium-based materials are prone to localized corrosion [34]. Moreover, it has been reported that 29 of 31 magnesium alloys suffer from localized corrosion [36]. Besides reacting with the human body environment, as explained previously, there are two other corrosion mechanisms that are threatening to magnesium implants. These two will be explained in the following.

Galvanic corrosion

Galvanic corrosion occurs when two different metals with different standard electrode potentials are in contact, and immersed in the same electrolyte. The less noble metal becomes the anode, and the more noble metal will become the cathode. A net flow will travel from the anode to the cathode, and hence the least noble metal becomes active and will corrode, while corrosion products will build up around the noble metal. The nobility of the metals is based on their ranking in the EMF-series. The larger the gap in standard electrode potentials between the two metals, the higher the corrosion rate will be [37].

When the circuit is under open conditions (no metallic contact between the two different metals), and equilibrium conditions are assumed, there exists a positive potential difference between the two metals, M and N, where N denotes the noble metal and M denotes the active metal [37]. The two different metals will stabilize at their equilibrium corrosion potentials, $E_{corr(M)}$ and $E_{corr(N)}$, and the difference in these potentials are ΔU as shown in Equation 2.5.

$$\Delta U = E_{corr(M)} - E_{corr(N)} > 0 \quad (2.5)$$

At closed circuit conditions, the two metals will be forced to stabilize at the same potential, known as E_{couple} , as in Equation 2.6 [38].

$$E_{corr(M)} = E_{corr(N)} = E_{couple} \quad (2.6)$$

To maintain E_{couple} a positive net current has to occur from the least noble metal to the noblest metal. The generation of a positive net current flow from N to M is a result of increased oxidation on the active metal N relative to its oxidation during open circuit conditions. Hence, the active metal will have a higher corrosion rate than before the galvanic coupling of the metals, and the noble metal will have a lower corrosion rate [38].

Magnesium is one of the most electrochemical metal in the electrochemical series and will, hence, almost always work as an anode. In the sense of biological corrosion, there are two considerations to be made concerning galvanic corrosion [1]. Firstly, if for instance fixation screws of another metal than magnesium are used for inserting a magnesium implant, these should be made of a material that lays close to magnesium in the electrochemical series to get the smallest possible corrosion rate. If there is a large gap in potential, as for instance with gold (Au) and magnesium, galvanic corrosion between them will occur, as demonstrated in Figure 2.1. Due to their difference in the EMF-series, the potential difference will drive electrons to flow from the magnesium implant (anode) to the gold screw (cathode), thus causing corrosion of magnesium.

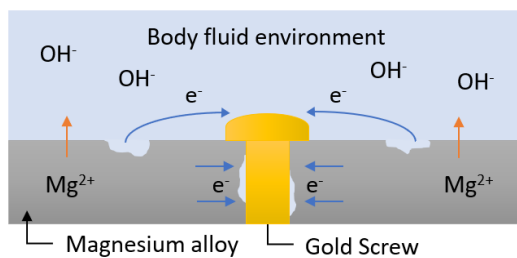


Figure 2.1: Galvanic corrosion between a gold fixation screw and a magnesium implant, revised from [1]. The gold fixation screw drives electrons from the magnesium implant due to their potential difference, causing corrosion.

The second consideration is concerning magnesium alloys, where impurities and second phases always are present. Because impurities and second phases normally

are cathodic with respect to the magnesium matrix, galvanic corrosion can occur between them. This is also called *microgalvanic corrosion* [37]. Microgalvanic corrosion on the surface of magnesium is illustrated in Figure 2.2, where the impurity and second phase will drive electrons from magnesium, thus dissolving the magnesium.

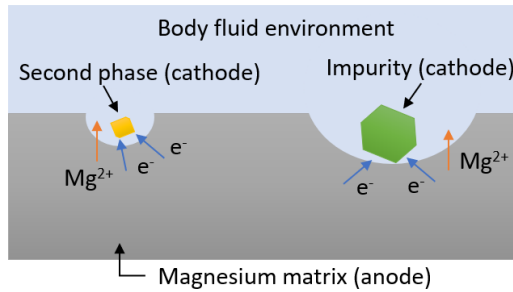


Figure 2.2: Galvanic corrosion between magnesium and second phases/ impurities elements, revised from [1]. The cathodic elements drives electrons from the Mg matrix, causing dissolution of the magnesium.

Pitting corrosion

Pitting corrosion occurs in small areas where the surface layer has been damaged locally. If the rest of the surface remains intact, this allows for corrosion to continue inwards the magnesium substrate through the damaged area. Galvanic corrosion between the magnesium matrix and the second phases/ impurities drives the corrosion further and creates pits with aggressive corrosive environments [27]. If the mouth of the pit is very small, the pit content may be hard to dilute, causing a high concentration of Mg^{2+} -ions. The positively charged ions will attract the negatively charged Cl-ions from the body fluid to neutralise the charge, which further accelerates the growth of the pit [39]. This is demonstrated in Figure 2.3. Once pitting starts, the process can be very rapid and hence causing early failure of an implant. When the implant is also exposed to stress or cyclic loading, *corrosion assisted cracking phenomenon* can occur, and the process will be even faster due to a local rise in stress created by the pit that will break the protective native layer [4]. Pitting corrosion is a kind of localized corrosion which can be hard to detect because corrosion products often cover the surface.

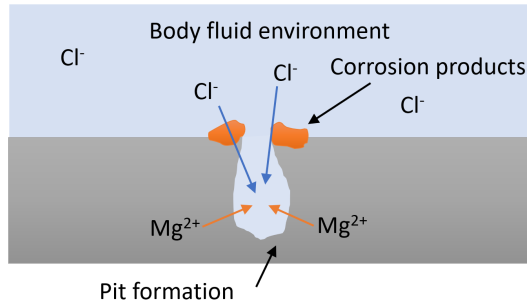


Figure 2.3: Pitting corrosion starting on the magnesium surface, revised from [1].
 The dissolution of magnesium inside the pit attracts Cl-ions to neutralise the charge, causing an aggressive corrosive environment inside the pit.

2.1.3 Corrosion challenges

The corrosion of magnesium for biomedical use is both the material's strength and weakness. So far, magnesium and its alloys are far from being a natural part of the applications on the biomedical field due to challenges that arise from their corrosion mechanism.

The first challenge is, as aforementioned, that the corrosion rate of magnesium is too high, causing the implant to fully degrade before the time of healing is completed [25]. The continuous degradation can also make it difficult to estimate the time of implant failure.

The second challenge involve the production of hydrogen gas during degradation, as seen in Equation 2.1. Hydrogen gas bubbles around the implant has been shown by several in vivo studies [25], and are one of the greatest concerns related to the use of magnesium in the human body. If the corrosion rate is too high, the human body will not be able to absorb all the evolved hydrogen, thus causing bubbles. The H₂-bubbles are harmful to the surrounding tissue in several ways; they can give a rise in pH in the surrounding body fluid, which can affect the pH-dependent physiological reactions in the area, or even lead to an alkaline poisoning effect [40], or cause necrosis in the surrounding tissue [26]. Furthermore, it was reported by E. Zhang [25] that a rise in pH can lead to bone absorption in undesired regions due to an accelerated deposition of calcium phosphate. In the same article it was reported that a rise in pH may induce hemolysis. The gas bubbles may also hinder cell adhesion due to a continuous fall out of corrosion products [41]. In worst case,

the H₂-bubbles can block the bloodstream, and cause the death of a patient [4]. Furthermore, the hydrogen evolution may lead to embrittlement of the implant due to the hydrogen embrittlement phenomenon [42]. This can induce the propagation of corrosion-assisted cracking phenomenon, again causing untimely failure of the implant [43]. Song [40] reported that the maximum tolerable hydrogen evolution rate is 0.01 mL/(cm² day), which correspond to a corrosion rate of 0.02mm/year, while Witte et. al [44] found that a hydrogen evolution of 0.068 mL/(cm² day) lead to an acceptable amount of hydrogen gas bubbles in guinea pigs after 2-3 weeks. However, it is not evident that these amounts will be tolerable in the human body.

2.1.4 Overcoming challenges

If magnesium is to be used in biomedical applications, the corrosion resistance evidently must be improved. There are different ways to achieve this, which will be presented in the following.

Reducing impurities

When second phases are present in the magnesium matrix, these accelerate the corrosion process due to the formation of microgalvanic cells. Due to the molten metal handling and the natural composition of magnesium, there are always impurities present in the material, as for instance Iron, Nickel, and Copper [45]. The solid solubility limit is the threshold below which an element can dissolve into a base material without forming a second phase [46]. Therefore, by keeping the impurities under their respective solid solubility limits, a single phase material can be ensured, thus reducing the corrosion rate. Indeed, it has been reported that the corrosion rate increases by 10-100 times [47] if the impurities are raised above their solid solubility limit. It is, therefore, crucial to keep the number of impurities at a minimum, as the tolerance levels for iron, copper, and nickel already are very low being 30-35ppm, 100-300ppm and 20-50ppm respectively [48]. However, these limits may change when there are alloying elements present in the magnesium matrix. For instance, Zinc and Manganese as alloying elements increase the tolerance limits due to the "Scavenger effect" [49]. Nevertheless, as for impurities, alloying elements have solid solubility limits which, if exceeded, will cause second phases.

Alloying

Alloying can improve the corrosion resistance with three different strategies, and these are described here as in [4].

1. Refining the grain size through alloying. The level of impurities and imperfections are higher along grain boundaries, due to higher internal energy in these areas than compared to the magnesium matrix. Because there is a segregation of second phases and alloying elements on the grain boundaries, corrosion usually occurs here. By refining the grain size, these segregations will be distributed through the whole magnesium substrate and the corrosion process will act more uniform than with coarse grains [22, 48]. Finer grains also hinder dislocation movement and can further hinder the propagation of cracks caused by corrosion assisted cracking phenomena.
2. Protecting the magnesium matrix by introducing passivating second phases. Passivating second phases can progress a protective film on the magnesium matrix and hence hinder corrosion.
3. By introducing alloying elements, precipitation of second phases at grain boundaries are reduced; the elements will help balance the potential difference between the matrix and the second phases.

Coatings

Alloying can decrease the general corrosion rate of a magnesium implant, but because many elements have low solubility in the Mg-matrix, sufficiently delaying the onset of degradation of magnesium is hard to obtain by alloying alone [28]. Also, alloying will not remove the galvanic corrosion problems which will occur if a magnesium implant is in contact with another metal and the same electrolyte [50]. Moreover, as magnesium alloys are quite soft, wear problems may occur if the surface is not protected [50]. Therefore surface treatment in terms of coatings is of high interest. A coating is an effective way to hinder corrosion, as it acts as a physical barrier for the corrosive environment. If the coating itself is stable in the surrounding environment, has good adhesion to the substrate, and is pore- and crack-free, the coating should completely protect the underlying substrate. However, an ideal coating is hard to obtain. The properties of the coating, such as thickness uniformity, conformality, adhesion, and number of pores or cracks, depend greatly the technique used to apply the coating. There are various coating techniques used for improving the corrosion resistance of magnesium, and

a literature study on conversion coatings, coatings by sol-gel process, physical vapor deposition (PVD), chemical vapor deposition (CVD), plasma electrolytic oxidation (PEO), and Atomic Layer deposition (ALD) is found in the specialization project prior to this thesis in Appendix A.

2.2 Atomic layer deposition

2.2.1 An introduction to the ALD-process

The coating technique atomic layer deposition, known as ALD, is based on chemical vapor deposition (CVD). ALD provides dense, thin, and conformal films that are built up by chemical reactions between two gaseous- or vapor phase precursors. The two precursors are brought into a reacting chamber alternating and separated [2]. Due to a limited number of reactive groups on the surface, the process is self-limiting. The chemical reactions are surface-reactions unlike gas-reactions, and hence ALD provides superior film uniformity [51]. The ALD-process can be divided into four steps [2, 52], which are illustrated in Figure 2.4:

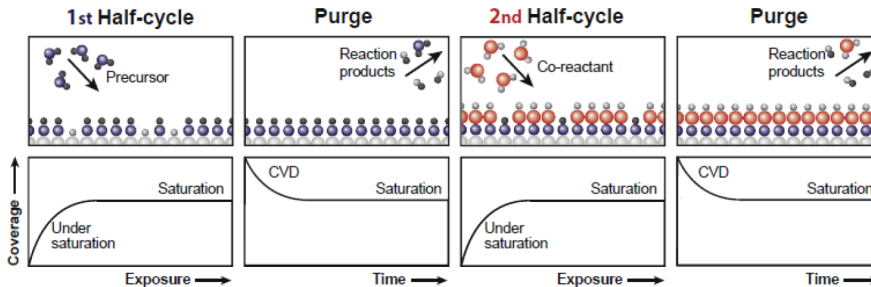


Figure 2.4: Illustration of the four steps in the atomic layer deposition process [2].

1. The main precursor is applied into the reactor chamber and is left until it has reacted with the available surface groups on the specimen. The precursor is often an inorganic coordination compound (a metal center with ligands).
2. The excess precursor is thereafter pumped or purged out of the reactor chamber by an inert gas, usually N_2 or Ar. This is an important step when the cycle is repeated to make sure that the precursor and co-reactant do not react with each other in the gas phase.

3. The second precursor, often a small molecule, is introduced when the system is cleared, which reacts with the molecules on the surface from the first precursor.
4. The system is then again purged or pumped.

This process, or cycle, deposits a monolayer on the substrate surface. To increase the thickness of the film, the cycle is repeated. For the process to work, it is crucial that the precursor and the co-reactant do not react with themselves nor the reaction products. This is to make sure that the reactions happen on the substrate surface, and that the process will be self-limiting in the sense that when the surface is saturated, the deposition stops [2].

2.2.2 ALD compared to other coating techniques

In the specialization project, found in Appendix A, prior to this thesis, a literature study on different coating techniques for improving the biocorrosion resistance of magnesium was done. The coating techniques studied were conversion coatings, coatings by sol-gel process, chemical vapor deposition (CVD), physical vapor deposition (PVD), plasma electrolytic oxidation (PEO) and ALD. The part in the specialization project where ALD is compared to other coating techniques, is revisited in this section.

When comparing the corrosion potential and current density results, from the atomic layer deposited coatings against the coatings prepared by other techniques, the results have no obvious gap in magnitude. Moreover, when comparing the thicknesses needed to achieve these results, nearly all coatings for other techniques have a coating at μm -scale in contrast to ALD-coatings where all coatings are at nm -scale. This indicates that less material is needed with ALD to achieve the desired protective properties.

As for degradation mechanisms, where it is desired to have a uniform coating to secure uniform corrosion, thickness control is an essential property for the coating technique. Additionally, since implant devices are characterized by notches and other geometrical discontinuities, the coatings ability to conformally coat the substrate is therefore highly claimed. For all three conversion coatings, anodizing and sol-gel techniques, the thickness is rather hard to control, hence giving a non-uniform surface. PEO, PVD and traditional CVD-methods provide better

thickness control than those just mentioned, but none is comparable to the conformal coatings created by ALD offering thickness control on atom level.

Biocompatibility highly depends on the composition of the coating rather than the technique. However, the choice of technique is important regarding coating composition control. All discussed coatings techniques offer composition control to some extent, with ALD being able to maximize it since it allows to stack monolayers on top of each other.

The primary motivation for applying a coating on magnesium alloys is corrosion protection, and hence, it is essential for the coating to completely cover the surface to avoid localized corrosion. For conversion coatings, both cracks and pores have been reported [50, 53], which may induce corrosion. Sol-gel coatings tend to crack upon drying [54] and therefore need to be carefully examined both before, during, and after drying. For PVD-films, inadequate long-term protection has been observed [55], and therefore a top-coat has often been applied to cover pores in the PVD-coating. This also goes for PEO-films, where discharges cause pores [29]; thus, a top-coat is very often necessary. In CVD-coatings the film is dense and smooth, in particular for ALD where the film is pinhole-free [52], which makes these techniques excellent corrosion inhibiting methods.

As magnesium is a heat-sensitive material [50], low processing temperature during film deposition is essential to avoid temperature defects such as phase transformations. ALD is not the only coating technique offering deposition at low temperatures but has its advantage in assuring good adhesion even at low temperatures. However, it should be emphasized that impurities in an ALD coatings are decreased with increased temperature [56]. PVD processing also offers low temperatures, but unfortunately, it is often difficult to control the temperature during deposition and to secure good enough adhesion to the substrate.

Although the properties of an ALD coating are superior in comparison to other techniques, it is noteworthy that ALD is time-demanding compared to other techniques due to low growth rates.

2.2.3 Magnesium and ALD

Even though ALD is an appropriate candidate for bio-corrosion protection of magnesium and magnesium alloys, there are few publications available on the field. To the best of this author's knowledge, there are less than ten articles who deal with ALD for corrosion protection of magnesium [57, 58, 59, 60, 61], while only two of these discuss the improvement of bio-corrosion resistance. In the specialization project these papers were reviewed, and a brief summary is given in the following.

Table 3: Results from polarization tests conducted on coatings prepared by ALD.

Alloy	Coating material	Thickness	Technique	Highest E_{corr} (V_{SCE})	Lowest i_{corr} (A/cm^2)	Test solution	Ref.
AZ31	ZrO ₂	11.7nm	Bare	-1.557	5.12×10^{-4}	0.9% NaCl	[62]
			ALD	-1.462	2.78×10^{-7}		
AZ31	PLGA/ ZrO ₂	- /11.7nm	Bare	-1.557	5.12×10^{-4}	0.9% NaCl	[62]
			Spin-coating/ALD	-1.452	4.90×10^{-9}		
Mg-Sr	ZrO ₂	38.8nm	Bare	-1.928	3.07×10^{-4}	SBF	[60]
			ALD	-1.75	4.88×10^{-6}		
AZ31	TiO ₂	100nm	Bare	1.48*	10^{-4}	0.05M NaCl	[59]
			ALD	-1.61	10^{-6}		
AZ31	Al ₂ O ₃	100nm	Bare	1.48*	10^{-4}	0.05M NaCl	[59]
			ALD	-1.46	10^{-6}		
AZ31	Al ₂ O ₃ / TiO ₂ /	100nm	Bare	1.48*	10^{-4}	0.05M NaCl	[59]
			ALD	-1.58	10^{-8}		
AZ31	Al ₂ O ₃ / TiO ₂ /	100nm	Bare	1.48*	10^{-4}	0.05M NaCl	[59]
			ALD	-1.57	10^{-8}		
AZ31	MgO and MgSiO ₄ / AZO	-/100nm	Bare	-1.561	3.16×10^{-4}	3.5wt% NaCl	[57]
			PEO/ALD	-0.550	1.36×10^{-6}		
Mg-Li	LiAl _x O _y	200nm	Bare	-1.46	2×10^{-3}	3.5wt% NaCl	[61]
			ALD	-1.08	10^{-4}		

*Reference electrode not SCE but Ag/AgCl

From Table 3 it can be seen that ALD-coatings lead to better corrosion resistance. This indicates that the thin, dense, and pinhole free coatings prepared by ALD are excellent considering corrosion protection. However, some articles reported about nano-gaps found in the coatings [57, 60], which allowed for the fluid to penetrate

through the coating. This was reported to be due to galvanic corrosion between the substrate and the coating and hence the corrosion performance was reduced. However, it was observed that by increasing the thickness of the deposited the film or adding a top-coat, the problem was minimized. Great results were also achieved by combining coatings [59]. Overall it can be concluded that there is a vast potential lying within ALD for the purpose of bio-corrosion protection of magnesium, but further investigation is necessary.

2.2.4 Biocompatible thin-films

In this master thesis, the coatings TiO_2 , ZrO_2 and HfO_2 prepared by ALD have been chosen due to their biocompatibility, chemical stability, and ease with ALD. TiO_2 is a stable coating both in chemically and physically, and exhibits super-hydrophilic properties [63]. It is also a common ALD-material for corrosion protection and is non-toxic for the human body [33]. The oxide has also been reported to have anti-bacterial properties [33]. ZrO_2 has many of the same properties as TiO_2 , being chemically stable and very wear-resistant [30]. ZrO_2 has also been shown to favor osseointegration and cytocompatibility [31]. HfO_2 , on the other hand, has not been evaluated for corrosion protection of magnesium but is an interesting candidate for CMOS-technology, and the ALD process is therefore well-known [64]. Nevertheless, Hafnium is in the same chemical group as Titanium and Zirconium, and was therefore expected to perform in a similar matter.

The corrosion resistance of amorphous structures has previously been reported to be excellent [65, 66]. As the deposition temperature of the ALD-coatings in this thesis was well below the crystallization temperature Zirconia, Hafnia and Titania [32], all oxides are expected to provide great corrosion protection. Additionally, the oxides are expected to be stable in the environment of Simulated body fluid (SBF).

2.3 Principles behind the experimental methods

2.3.1 Potentiodynamic polarisation tests

The aim of potentiodynamic polarisation tests is to achieve the corrosion potential (E_{corr}) and the corrosion current density (i_{corr}). The corrosion current density is simply the corrosion current divided by the area. These are of interest because the corrosion potential indicates corrosion resistance and, more importantly, the corrosion current density is linked to corrosion rate by the Equations 2.7-2.11 [67], starting with Faraday's law as in Equation 2.7.

$$I = nFN \quad (2.7)$$

where

I = partial current due to charge transfer reaction (A)

F = Faraday's constant (96487 Cmol⁻¹)

N = number of moles of metal/reactant oxidized or reduced per second (mol s⁻¹)

n = number of electrons transferred by the charge transfer reaction (mol⁻¹)

For the oxidation process that takes place on the metal, Faraday's law can be written in the form showed in Equation 2.8.

$$I_{ox} = nFN_{ox} = I_{corr} \quad (2.8)$$

Furthermore, the corrosion rate is often referred to by the weight loss, as given in Equation 2.9.

$$\frac{dW}{dt} = N_{ox}W_o \quad (2.9)$$

where

$dW/dt = \text{rate of weight loss (corrosion rate) (gs}^{-1}\text{)}$

$W_0 = \text{molecular weight of corroding material (gmol}^{-1}\text{)}$

By substitution and integration over a period of t seconds, where Q is the total amount of charges exchanged in coulombs during time t , we obtain the expression for total weight loss, W , in Equation 2.10

$$W = \frac{W_0}{nF} \int_0^t I_{ox} dt = \frac{W_0 Q}{nF} \quad (2.10)$$

The corrosion rate - or weight loss - is more important than the total weight loss, and we obtain the expression in Equation 2.11.

$$\text{Loss of thickness (cm/s)} = \frac{1}{\rho A} \frac{dW}{dt} = \frac{I_{corr} W_0}{\rho A n F} = \frac{i_{corr} W_0}{\rho n F} \quad (2.11)$$

Hence, the thickness loss can be determined by the current density. The relation of corrosion current density and corrosion potential is described in the following paragraphs.

When a corrosion process takes place on a metal surface, two electrochemical processes are happening: an anodic reaction and a cathodic reaction. During this process the anode releases electrons (I_a) which are consumed by the cathode (I_c), thus the corrosion current, or corrosion rate, will be determined by the slowest of these processes as according to Equation 2.12 [68].

$$I_a = I_c = I_{corr} \quad (2.12)$$

The anodic and cathodic reactions are both characterized by different equilibrium potentials ($E_{eq,c/a}$). The corrosion potential E_{corr} is determined as the driving voltage ΔE (Equation 2.13), which equals the sum of dissipations or absolute values of overvoltage happening on the anode and the cathode, η_a and η_c [3].

$$\Delta E = E_{eq,c} - E_{eq,a} = E_{eq,H_2} - E_{eq,Me} = \eta_a + |\eta_c| \quad (2.13)$$

This is clearly shown in an Evan's diagram, which plots potential vs. current density. The diagram shows how the potential changes depending on the variations in current density, as shown in Figure 2.5. The lines in the Evan's diagram follows the Tafel equation, as in Equation 2.14 and 2.15, who describes the relationship between the electrode potential and the partial current of a charge transfer reaction of the anodic and cathodic reactions, respectively [3]. Hence, the current density and corrosion potential can be read off at the intersection point of the polarisation curves of the anodic and the cathodic process.

$$\eta_a = a + b \log i = b \log\left(\frac{i}{i_0}\right) \quad (2.14)$$

$$\eta_c = -a - b \log i = -b \log\left(\frac{i}{i_0}\right) \quad (2.15)$$

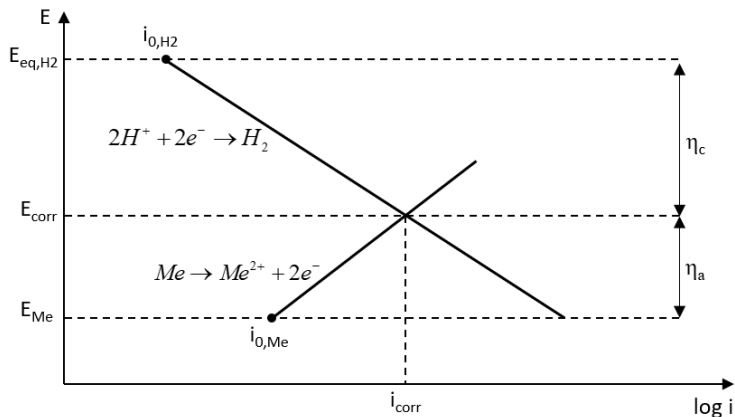


Figure 2.5: Evan's diagram for a metal (Me), revised from [3].

However, the lines depicted in Evan's diagrams are theoretical lines, and polarization curves can only be obtained experimentally. To measure the two values corrosion potential (E_{corr}) and the current density (i_{corr}), the polarisation- or overvoltage curves of the anodic and cathodic reactions must firstly be plotted. The polarisation curves can be obtained either by imposing current or by imposing the potential. When using a potentiodynamic method, potential is imposed with the help of a potentiostat. The potentiostat increases the potential of the working electrode continuously starting at a fixed value, usually the open circuit potential. In this way, the potentiodynamic method act as a corrosion

process where the driving voltage determines the corrosion current [3]. The corrosion potential and corrosion current density are then obtained by identifying the linear Tafel regions, and drawing Tafel lines onto the polarization curves and reading of at the intersection of these two, as illustrated in Figure 2.6.

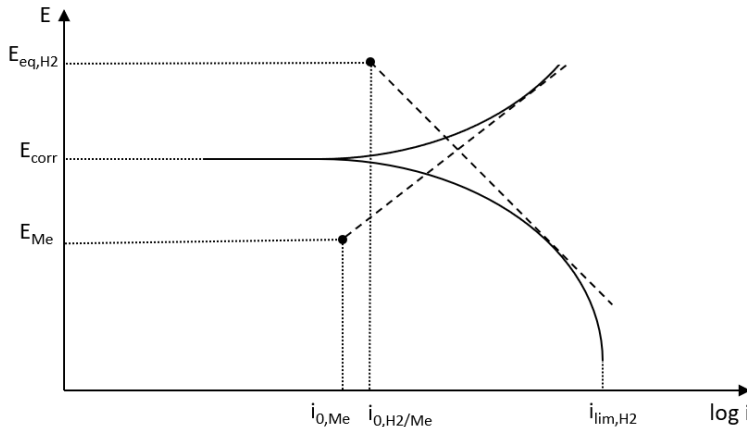


Figure 2.6: The dotted lines shows the theoretical Tafel lines and the solid lines shows the experimental polarisation curves (For an active metal (Me) in an oxygen-free acidic solution). Revised from [3].

The set-up for a potentiodynamic polarisation experiment has a standard three-electrode configuration; The test sample is the so-called working electrode and becomes an anode. A counter electrode, a nobler material than the test sample, works as a cathode. Additionally, a reference electrode with a known electrode potential is set up to scope the potential of the working electrode.

2.3.2 Electrochemical Impedance Spectroscopy

Electrochemical impedance spectroscopy (EIS) is a popular tool for corrosion studies as it can measure and separate the electric and dielectric properties of individual contributors of components under investigation [69]. The technique measures the impedance of a system over a wide frequency range. The impedance is measured by applying an AC potential and then measuring the corresponding current. The mathematical approach is based on Ohm's law, where there is a linear relation between potential and current. Nevertheless, the relation between potential and current in electrochemical systems is usually non-linear. However, in a range of 5-10 mV, it is possible to approximate this relation as linear, and

hence, EIS is applied within this potential range [70]. When a sinusoidal potential is applied in a linear system, the current response will also be sinusoidal and at the same frequency only shifted in phase. The system impedance (Z) is shown in Equation 2.16, where ω is the radial frequency of $2\pi f$ and ϕ is the phase shift [70]. E_0 and I_0 denotes the amplitude of potential and current.

$$Z = \frac{E(t)}{I(t)} = \frac{|E_0|\sin(\omega t)}{|I_0|\sin(\omega t - \phi)} = Z_0 \frac{\sin(\omega t)}{\sin(\omega t - \phi)} \quad (2.16)$$

In the following paragraphs, the concept of EIS is described as in [71]. The impedance is often expressed by a complex function with a real and imaginary part (Equation 2.17). In electrochemistry the real and imaginary parts are often marked as Z' and Z'' , respectively.

$$Z(\omega) = Z_0(\cos\phi + j\sin\phi) = Z_{Re} + jZ_{Im} \quad (2.17)$$

Thus, the modulus of impedance, $\tan\phi$ and the shift angle ϕ , can be expressed as following equations, 2.18, 2.19 and 2.20.

$$|Z(\omega)| = \sqrt{Z_{Re}^2 + Z_{Im}^2} \quad (2.18)$$

$$\tan\phi = \frac{Z_{Im}}{Z_{Re}} \quad (2.19)$$

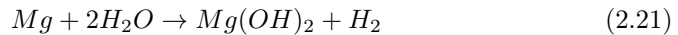
$$\phi = \arctan \frac{Z_{Im}}{Z_{Re}} \quad (2.20)$$

When analyzing EIS-data, both Nyquist- or Bode-plots are used as they complement each other in regards to weaknesses the plots have alone. In Nyquist-plots the real (Z') and imaginary part (Z'') are plotted against each other and are often formed as a semicircle. With this plot, effects of the ohmic resistance are seen, and it considers the different circuit components in the series. In Bode-plots on the other hand, one plots $|Z(\omega)|$ and ϕ against $\log\omega$ and examines these as functions of frequency. The data in both plots are analyzed by fitting the data to an electrical circuit consisting of elements such as resistors,

capacitors, and inductors, which each represent a physical meaning in the electrochemical process. These elements are passive and do not generate current or potential. [69]

2.3.3 Hydrogen evolution

As stressed earlier, a rapid hydrogen evolution during the degradation of a magnesium implant can harm the patient. Therefore monitoring and measuring the hydrogen evolved during corrosion of magnesium is important. Also, as explained before, when magnesium is immersed in an aqueous solution, magnesium will react with water as according to equation 2.21.



As reported in equation 2.21, for each mole of magnesium which is consumed, one mole of hydrogen gas is produced. Therefore, by measuring the hydrogen gas, the mass loss of magnesium, and hence the corrosion rate can also be measured. In comparison to traditional weight loss methods, this method gives the opportunity of monitoring the corrosion rate from day to day. Moreover, for traditional weight loss methods, the corrosion products must be removed, and hence there is a risk of removing not only the coating, but also the magnesium itself. This is avoided when measuring hydrogen evolution.

For magnesium alloys, the corrosion process might be believed to be more complicated due to the microstructural constituents in the alloy. However, the matrix α -phase in magnesium will always corrode firstly, and the α -phase in AZ-alloys has been shown to corrode in the same manner as pure magnesium [72]. Hence, this is a suitable method to measure both hydrogen evolution and corrosion rate.

3 Experimental Procedure

3.1 Materials

Magnesium alloy AZ31 has been used in all experiments. This is an aluminum-containing alloy with aluminum and zinc as main alloying elements. The nominal composition of AZ31 is 3% Al, 1% Zn, and 0.3% Mn [73].

3.2 Sample preparation

All AZ31 samples were mechanically polished down to P2000 grit. The samples for the potentiodynamic polarization tests and EIS were circular with a thickness of about 2 mm and a diameter of 24 mm, while the samples for the hydrogen evolution experiments were cut to cubes of about 10 x 10 x 6 mm. After grinding, the samples were rinsed ultrasonically with acetone and ethanol both for 5 minutes. Right before the deposition of coatings onto the samples, all samples were plasma cleaned with Argon-gas for 20 minutes.

3.3 Atomic layer deposition

Coatings were deposited by the ALD technique as described earlier, by the ALD-reactor (Savannah S200, Veeco Instruments Inc., Massachusetts, USA). The precursors for oxygen, zirconium, hafnium, and titanium were H₂O (water vapor), Tetrakis(Dimethylamido)Zirconium, Tetrakis(Dimethylamido)Hafnium and Tetrakis(Dimethylamido)Titanium, respectively. Depositions were executed at 160 degrees Celsius with N₂ as the carrier gas.

In advance of the deposition of the test samples, deposition on 100 mm Silicon (<100>, b-doped) wafers (J14014, Siegert Wafer GmbH, Aachen, Germany) was done in order to find the deposition rate. Before depositing on the wafers, they were plasma cleaned, and then hydroxylated with 10 cycles of H₂O in the ALD reactor. After deposition, the thickness was divided by the number of cycles to estimate the growth rate. Thereafter, the number of cycles were carefully chosen for each coating in order to obtain thicknesses of about 100 nm. The thickness was measured by spectroscopic ellipsometry (M-2000, J.A Woollam Co., USA). The

resulting thicknesses, with corresponding cycles, can be seen in Table 4.

Table 4: Thickness and number of cycles for the different coatings.

Coating material	Number of cycles	Thickness
HfO ₂	826	112 nm
ZrO ₂	926	122 nm
TiO ₂	1980	100-120 nm

3.4 Scanning Electron Microscopy

The bare and coated surfaces, before and after potentiodynamic polarisation testing, was examined in a Scanning Electron Microscope (SEM) (Quanta FEG 650, FEI Company, Oregon, USA). The working distance was about 10 mm, and the acceleration voltage was set to 20 kV.

3.5 Electrolyte

As when inserting a foreign object, such as an implant, into the body, the response of the human body is unknown. Hence, testing in vitro is essential. Therefore a fluid that can represent the in-body-environment is needed, which in this master thesis was "Simulated body fluid" (SBF). The SBF was created after the recipe in [74], and the ion concentration of SBF compared to blood plasma can be seen in Table 5.

Table 5: The ion-concentration of SBF compared to blood plasma.

Ion	Ion concentration (mM)	
	Blood plasma	SBF
Na ⁺	142.0	142.0
K ⁺	5.0	5.0
Mg ²⁺	2.5	2.5
Ca ²⁺	1.5	1.5
Cl ⁻	103.0	147.8
HCO ₃ ⁻	27.0	4.2
HPO ₄ ²⁻	1.0	1.0
SO ₄ ²⁻	0.5	0.5
pH	7.2-7.4	7.40

3.6 Test set-ups

3.6.1 Potentiodynamic polarization curves

The potentiodynamic polarization curves was measured using potentiostat (Interface1000, Gamry instruments, Pennsylvania, USA), and carried out in a cell containing around 100 mL of SBF. The cell is shown in Figure 3.1. The set-up consisted of a typical three-electrode configuration, with the sample being the working electrode, Palladium as the reference electrode, and Hg/Hg₂SO₄ as the counter electrode. All tests were conducted at room temperature. Prior to the polarization tests, the samples were kept in the solution for 30 minutes to obtain the open circuit potential (OCP) and to stabilize in the solution. Thereafter, the electrode potential was raised from -2 V to 2 V relative to the OCP at a sweeping rate of 0.5 mV/s.

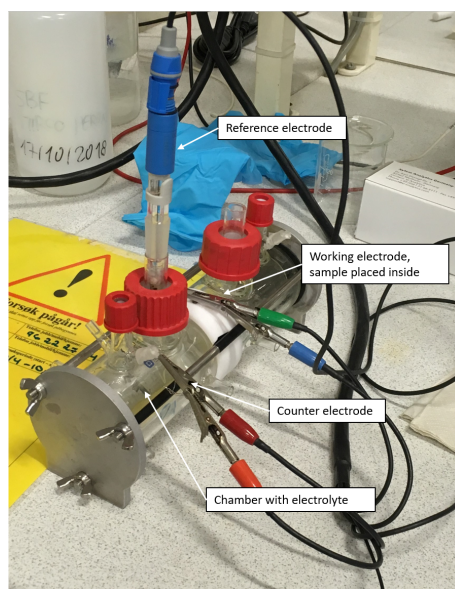


Figure 3.1: Set-up for the potentiodynamic polarisation tests.

The values of corrosion potentials (E_{corr}) were obtained by reading off the value at the point where the anodic and the cathodic polarization curves stabilize. The values for current density (i_{corr}) was obtained by extrapolating the Tafel lines of the anodic and cathodic polarization curves. For each sample, the experiment was repeated three times to assure results reproducibility.

3.6.2 Electrochemical Impedance Spectroscopy

Electrochemical impedance spectroscopy was carried out using the same three-electrode configuration and the same potentiostat, as described in Section 3.6.1. Additionally, the electrochemical cell was placed inside a Faraday's cage to avoid noise in the results. For fitting of the results, the software "Gamry Echem Analyst" was used. The signal amplitude during EIS was 10 mV relative to the OCP at a frequency range of 10^{-2} to 10^5 Hz. The samples were kept in SBF for 30 minutes before measurements to stabilize and to measure OCP. For each sample, the experiment was repeated three times to assure results reproducibility.

3.6.3 Hydrogen evolution

The hydrogen evolution experiment was set up as described in [75]. The set-up is illustrated in Figure 3.2. A test sample was placed under a funnel, which ensured that all evolved hydrogen would be trapped. Thereafter a burette filled with SBF was mounted on top of the funnel. The burette was closed at the top so that all H_2 -gas trapped by the funnel would be collected in the burette. Moreover, when set up this way, the evolved gas gradually pushed the SBF downwards in the burette allowing for reading of how many mL of gas had been evolved each day. One experiment lasted a week at room temperature, and measurements were made at the same time each day that week. For each sample, the experiment was repeated three times to assure results reproducibility.

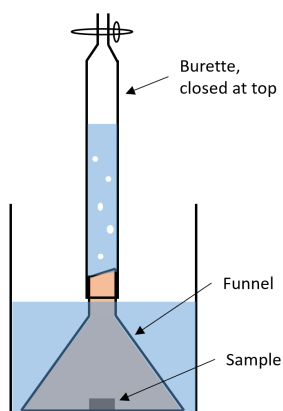


Figure 3.2: Schematic illustration of the hydrogen evolution experiment.

4 Results

4.1 Surface characterization

In Figure 4.1, SEM-pictures of bare and coated samples are shown. As seen in Figure 4.1a, where the bare sample is shown, there are several scratches on the surface from the mechanical polishing. These scratches are also evident in Figure 4.1b, 4.1c and 4.1d, where the coated samples are shown, indicating thin and conformal coatings.

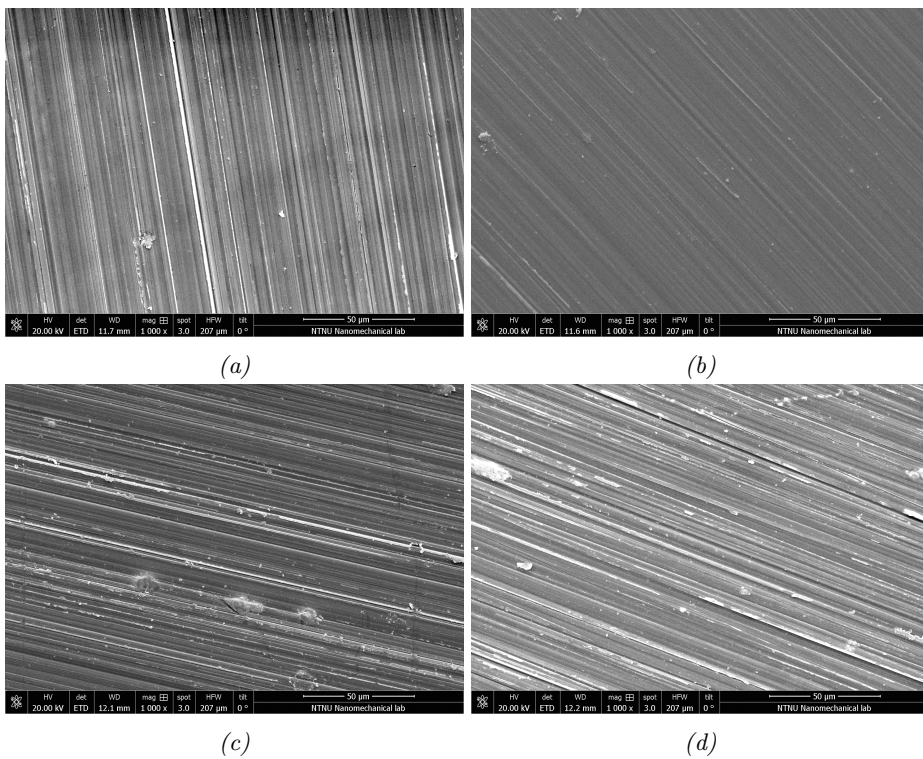


Figure 4.1: SEM-pictures of different AZ31-samples where (a) Untreated (b) Coated with ZrO_2 (c) Coated with HfO_2 (d) Coated with TiO_2

4.2 Potentiodynamic polarization curves

In Figure 4.2, the average potentiodynamic polarisation curves for the different samples in SBF are plotted against each other. In Figure 4.3, a close up of Figure 4.2 are shown. The results from these tests are shown in Table 6. The curves for each different test can be found in Appendix B. A lower value for corrosion current density indicates a lower corrosion rate and, hence, an improvement in corrosion performance. For corrosion potential, on the other hand, a higher value indicates the material becoming less prone to corrosion.

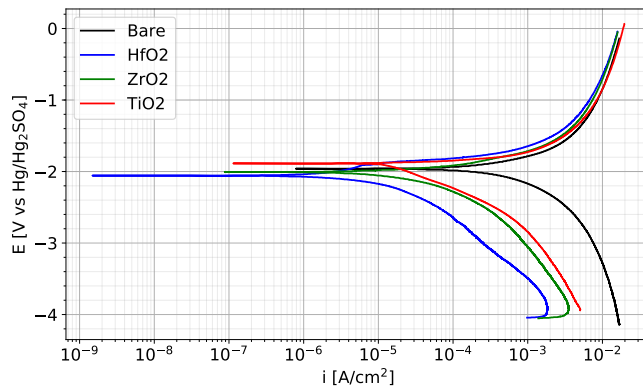


Figure 4.2: Potentiodynamic polarisation curves for coated and bare samples in SBF.

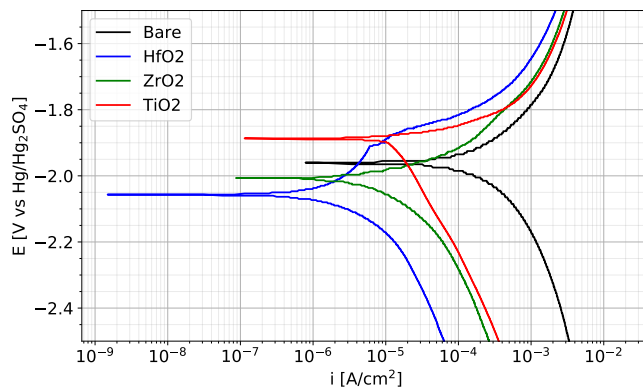


Figure 4.3: Potentiodynamic polarisation curves for coated and bare samples in SBF, close up of Figure 4.2.

Table 6: Corrosion potential and corrosion current density of the bare and coated samples.

	E_{corr} [V _{Hg/Hg₂SO₄}]	i_{corr} [A/cm ²]
Bare	-1.95	$\sim 10^{-4}$
HfO ₂	-2.05	$\sim 10^{-7}$
ZrO ₂	-2.01	$\sim 10^{-6}$
TiO ₂	-1.89	$\sim 10^{-5}$

Regarding i_{corr} , the tested samples can be placed in the following rank HfO₂ > ZrO₂ > TiO₂ > Bare, where HfO₂ has the lowest current density and the bare sample has the highest. All the coatings reduced the corrosion current density substantially, as seen in Table 6, thus indicating that the coatings have a significant effect on this value. The values for the corrosion potential, E_{corr} , on the other hand, are very similar to each other, indicating that the coatings have little effect on the corrosion potential.

The samples after the potentiodynamic polarisation tests are shown in Figure 4.4. On the bare sample, visually uniform corrosion products covered the whole surface. For the samples coated with ZrO₂, HfO₂ and TiO₂, the corrosion products did not cover the entire surface, but rather formed in heaps or dots on the surface, as seen in Figure 4.4b), c) and d). In Figure 4.5, the samples are cleaned with chromic acid, and the figure shows SEM-images of the corroded parts. For all samples, both treated and untreated one, pits are seen in the corroded area.

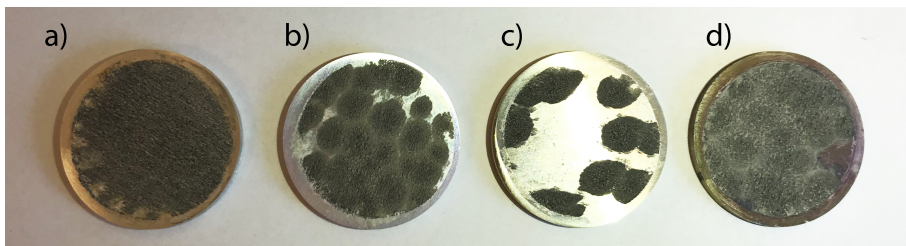


Figure 4.4: Samples after potentiodynamic polarisation testing where (a) Bare (b) Coated with ZrO₂ (c) Coated with HfO₂ and (d) Coated with TiO₂.

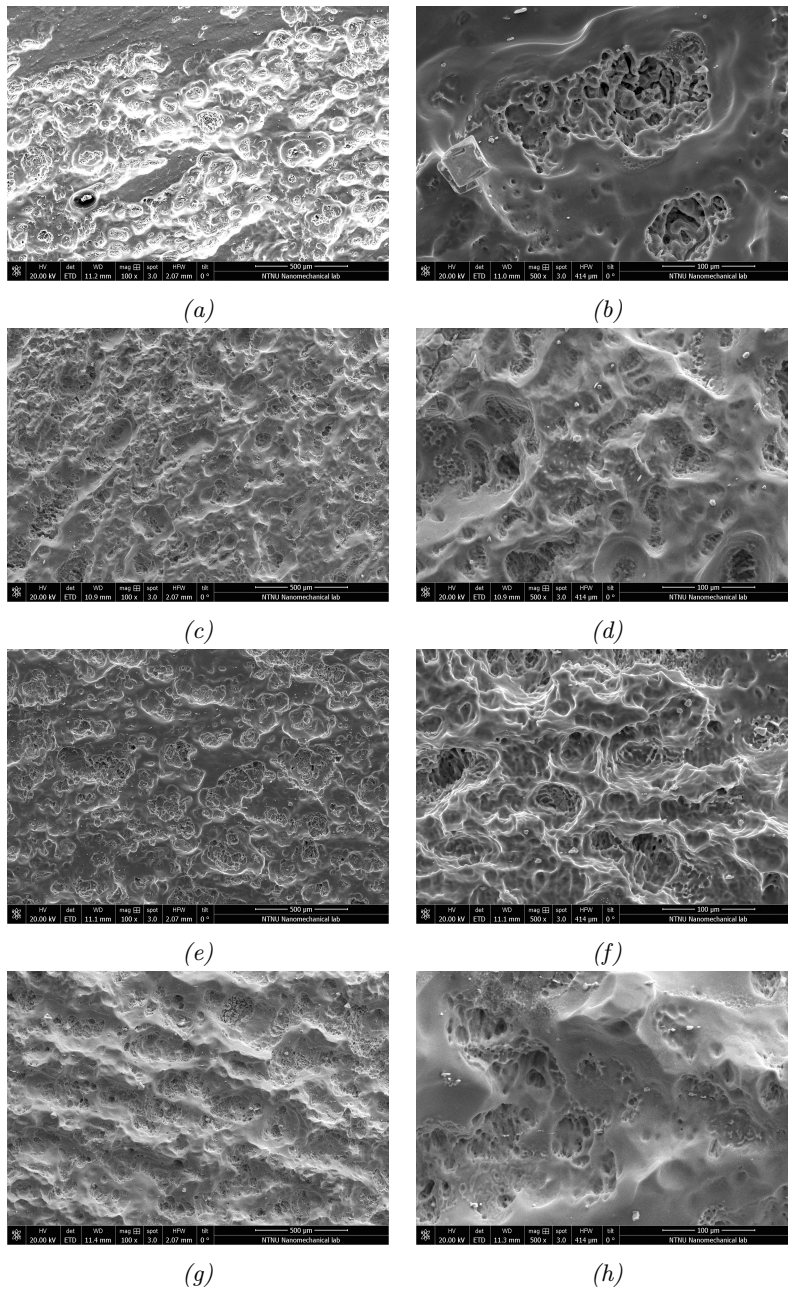


Figure 4.5: SEM-images of samples after potentiodynamic polarisation tests, where (a) Bare (b) Magnification of a (c) ZrO_2 -coated (d) Magnification of c (e) HfO_2 -coated (f) Magnification of e (g) TiO_2 -coated (h) Magnification of g.

4.3 Electrochemical impedance spectroscopy

The Nyquist-plots are shown in Figure 4.6. In the Nyquist plots, the bare sample and the coated samples are characterized by three time constants being the capacitive loop in the high and medium frequency range, and the inductive loop in the low-frequency range [76, 77]. The capacity loop is connected to the transfer process between the coating and the substrate, while the inductive loop describes the corrosion of AZ31 [76, 77]. A larger capacitive loop means better corrosion resistance [60]. Due to the larger diameter of the capacitive loops of the coated samples compared to the bare sample, the treated samples show much better performance in corrosion resistance. The diameter of the capacitive loops, and hence, the corrosion performance is ranked $\text{HfO}_2 > \text{ZrO}_2 > \text{TiO}_2 > \text{Bare}$. There is a large difference in impedance among the different samples, as can be seen by inspecting the order of magnitudes on the axes.

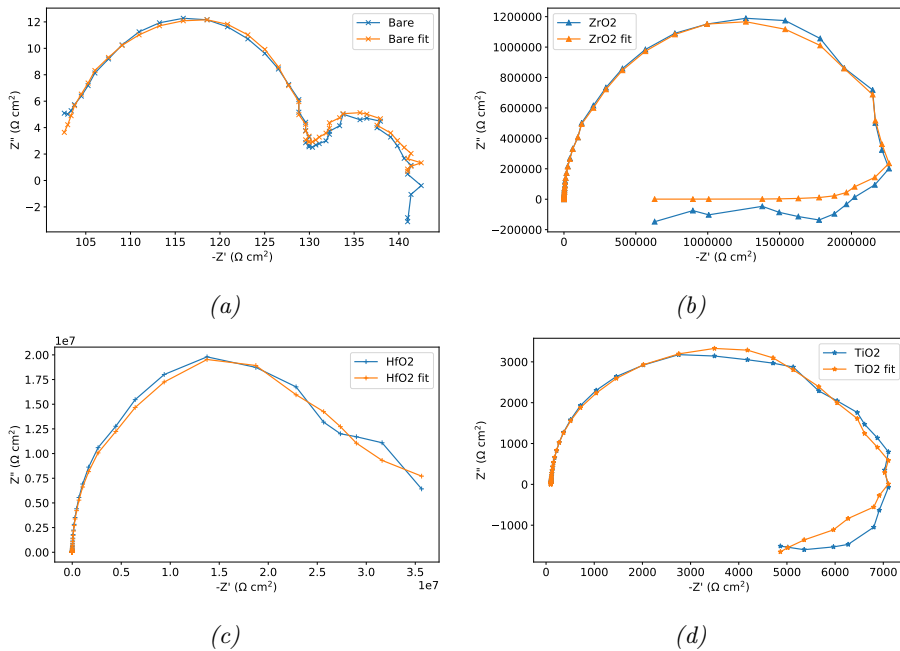


Figure 4.6: Nyquist plots for the different samples a) Bare b) Coated with ZrO_2 c) Coated with HfO_2 d) Coated with TiO_2 .

The Bode plots are shown in 4.7. The Bode plots also help to investigate the corrosion resistance as a higher value of $|Z|_{f \rightarrow 0}$ means greater corrosion resistance

[78, 79]. The $|Z|_{f \rightarrow 0}$ -value for the bare sample, the ZrO_2 -coated sample, the HfO_2 -coated sample and the TiO_2 sample is $1.4 \times 10^2 \Omega\text{cm}^2$, $7 \times 10^5 \Omega\text{cm}^2$, $4 \times 10^7 \Omega\text{cm}^2$ and $5 \times 10^3 \Omega\text{cm}^2$ respectively.

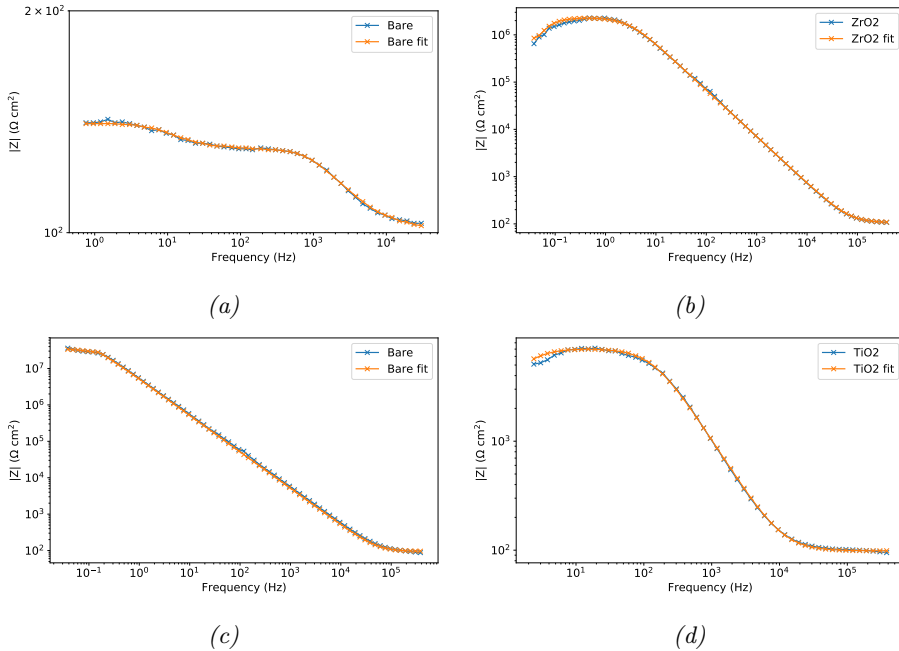


Figure 4.7: Bode plots for the different samples a) Bare b) Coated with ZrO_2 c) Coated with HfO_2 d) Coated with TiO_2 .

The EIS spectra can be simulated by an equivalent circuit, and the one used for fitting the EIS data is shown Figure 4.8. This equivalent circuit has been taken from literature where ALD-films for the same purpose as discussed in this thesis have been investigated [60, 62, 80]. The fitting results are shown in Table 7. Here, R_s , R_1 and R_2 represent the electrical impedance of the electrolyte, the surface modification layer (MgO), and the charge transfer resistance respectively. C_1 represents the capacitance of either the coatings or the surface corrosion products of the bare AZ31 [62]. R_L and L represent the resistance and inductance of the species absorbed into the coating, respectively [81]. Q_1 acts as a constant phase element (CPE) of the electric double layer on the electrode surface [60]. All the coated samples exhibit higher values for R_1 and R_2 , and lower values for Q_1 and C_1 , compared to the untreated sample. This indicates successful deposition of the coatings and higher corrosion resistance.

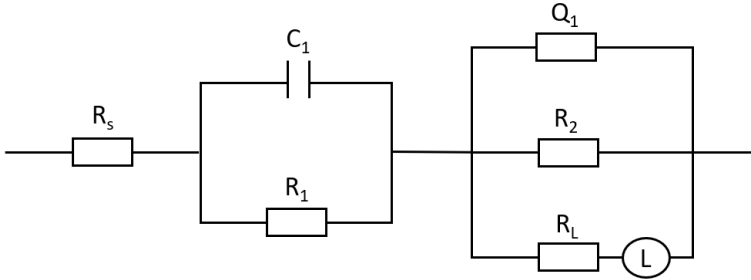


Figure 4.8: Equivalent circuit for EIS.

Table 7: Fitting results for EIS.

	Bare	ZrO2	HfO2	TiO2
R_s ($\Omega \text{ cm}^2$)	100,16	106,40	95,00	98,42
R_1 ($\Omega \text{ cm}^2$)	9,34	$1,64 \times 10^{11}$	$3,30 \times 10^7$	$2,63 \times 10^3$
C_1 ($\Omega^{-1} \text{ cm}^{-2} \text{ s}^{-n}$)	$5,71 \times 10^{-3}$	$1,05 \times 10^{-5}$	$1,29 \times 10^{-7}$	$1,29 \times 10^{-4}$
Q_1 ($\Omega^{-1} \text{ cm}^{-2} \text{ s}^{-n}$)	$7,07 \times 10^{-5}$	$9,71 \times 10^{-8}$	$1,30 \times 10^{-6}$	$7,24 \times 10^{-7}$
n	0,7479	0,984	0,999	0,938
R_2 ($\Omega \text{ cm}^2$)	$3,79 \times 10^1$	$2,25 \times 10^6$	$3,80 \times 10^7$	$6,88 \times 10^3$
R_L ($\Omega \text{ cm}^2$)	$1,78 \times 10^2$	$3,21 \times 10^{-1}$	$1,71 \times 10^6$	$1,05 \times 10^3$
L (H cm^2)	$1,84 \times 10^{-1}$	$2,42 \times 10^7$	$1,25 \times 10^7$	$2,35 \times 10^{-3}$

4.4 Hydrogen evolution

In Figure 4.9, the hydrogen evolution results for different AZ31 samples immersed in SBF for seven days are shown. The sample clearly evolving the most hydrogen gas for the entire period is the bare sample. The untreated sample has the fastest evolution rate at the beginning and throughout the immersion period. However, the Titania sample evolves no hydrogen after 24 hours, but after two days, this sample evolves at more or less the same rate as the bare one. In contrast to the Titania-sample, the Hafnia-sample corrodes during the first 24 hours, but despite this, the corrosion rate is kept lower than the former for the whole period of immersion. The Zirconia-sample is the most stable sample, staying inert for for the first 3 days before evolving from day 3-6, and then stabilize again on day 6.

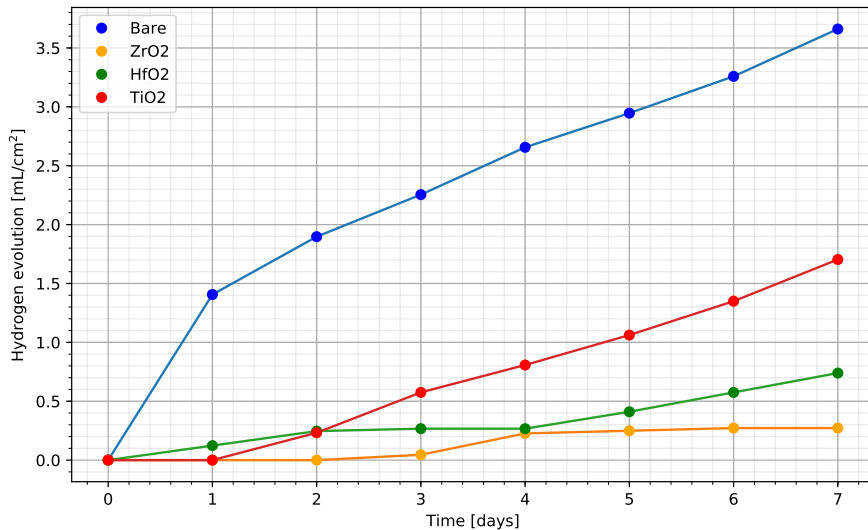


Figure 4.9: Hydrogen evolution of different AZ31 samples.

5 Discussion

5.1 Corrosion mechanism of the ALD-coated magnesium alloy AZ31

By the work done in this master thesis, it is evident that coatings prepared by ALD can delay the corrosion of alloy AZ31 to some extent. However, if the coatings completely covered the magnesium surface, no fluid could, in theory, reach the surface, and hence no corrosion of the magnesium surface would occur. Nevertheless, when the coated AZ31-substrates was tested electrochemically, and immersed to measure hydrogen evolution, corrosion of the magnesium alloy occurred. Therefore, the coatings cannot have been fully dense as the electrolyte must have penetrated through the coatings.

As previously reported about ZrO_2 -coatings prepared by ALD [58, 60], there exist some nanometer gaps between the deposited atoms in the deposited film. It is likely that this also is the case for the coatings prepared in this thesis. The gaps cause the SBF to penetrate the coating and reaching the bare magnesium surface. Furthermore, the reaction between magnesium and water produces hydrogen gas, in which locally damage the coatings and expose a wider area of bare magnesium.

The argument of gaps present in the coatings is in agreement with the potentiodynamic polarisation tests. If the coating had been uniform, this would indicate that it was the coating that degraded, and not the Mg substrate, however, this was not the case. In Figure 4.4 in Section 4, it can be seen that the corrosion products gathered in piles, and in Figure 4.1 it can be seen that pitting corrosion was the main corrosion mode. Thus, the corrosion was local before spreading across the sample surfaces, which indicate defects in the coatings.

Nevertheless, in the hydrogen evolution experiment, a large percentage of the Hafnia-, and Zirconia coated surface on the cubic samples appeared untouched after the period of immersion, except for some pits. Zirconia was the most stable coating throughout the immersion period, while the hydrogen evolution of Hafnia increases significantly from day 4. The former may be due to the aggressive corrosive environment formed in the pits. The corrosion in the pits was may accelerated by galvanic differences between the elements in the alloy [82]. In alloy AZ31, Aluminum and Zinc are the main elements, and as seen in Table 2 in

Section 1, the standard electrode potential for Al, Zn and Mg are -1.66 V, -0.76 V and -2.37 V, respectively. Thus, Mg will always be the anode. Additionally could the chloride environment, and the Mg-ions from anodic dissolution further have accelerated the corrosion [82].

Moreover, the stabilization of the Hafnia- and Zirconia samples on day 2-4 and 4-7, respectively, may be because corrosion products covered the pits, hindering corrosion or the release of hydrogen gas. On the Titania-sample, on the other hand, large corroded areas were observed, indicating more defects in this coating, leading to a corrosion rate similar to that of the bare sample already from day 2.

5.2 Comparison of coating performance on AZ31

The potentiodynamic polarisation results showed that all coatings lowered the corrosion current density by more than one decade. The bare sample had a current density of about 10^{-4} A/cm² while the best performing coating, Hafnia, had a current density of approximately 10^{-7} A/cm². Secondly came Zirconia, lowering the current density to about 10^{-6} A/cm², while Titania decreased the current density to around 10^{-5} A/cm². The EIS results agreed to this ranking. In the Nyquist-plots, the capacitive loop of Hafnia was bigger than the Zirconia-loop by a decade and bigger than the Titania loop by four decades. Also did the $|Z|_{f \rightarrow 0}$ -values from the Bode-plots, and C_1 -values suggest that Hafnia had the best corrosion resistance. However, the results from the hydrogen evolution experiments were contradicting to the former. These results showed that the Zirconia sample was the most protective coating.

Therefore, the coatings can overall be ranked in corrosion resistance performance by $\text{HfO}_2 \approx \text{ZrO}_2 > \text{TiO}_2$. Titania being ranked the poorest of the three coatings may be attributed to the low growth rate of the oxide. To obtain a thickness of around 100 nm, more than twice as many cycles for Titania (1980 cycles) were needed compared to Hafnia (826 cycles) and Zirconia (926 cycles). When the number of cycles increases, the size of the deposited nanoparticles decreases slightly [60]. Moreover, when particles decrease in size, the nanometer gaps between the particles will increase. Therefore, Titania may have larger gaps in the coating, leading to a more rapid penetration compared to Zirconia and Hafnia.

5.3 Coating thickness

A coating thickness of at least 10 nm is required for the deposited coating to have a protective effect [83]. The coating thicknesses were chosen based on the results found in the specialization project, as summarized in Section 2.2.3. Because some papers [58, 60, 61] reported that increasing the thickness would increase the protective properties by making up for imperfections, such as gaps, in the coatings, coatings-thicknesses of around 100 nm were chosen on this hypothesis. However, as observed, the coatings are not completely protective of the AZ31-samples. Kääriäinen et al. [84] reported that ALD-thickness above 100 nm might form cracks that reduce the barrier properties of the coating. Moreover, for the coatings prepared in this thesis, all film thicknesses exceeded 100 nm. Therefore there might have been not only nanometer gaps due to deposition but also cracks due to thickness reducing the coating performance. However, the thicknesses of the coatings were measured to 112 nm, 122 nm, and between 100-120 nm for Hafnia, Zirconia, and Titania respectively, whereas the thickest coating, Zirconia, also was the coating that showed best protective properties in the hydrogen evolution experiment, where the samples were immersed in SBF for 7 days. This may indicate that the Zirconia coating was the coating with the least defects. Thus, the observation by Kääriäinen et al. was not the case for the coatings prepared in this thesis.

5.4 Biocompatibility of ALD-coatings

The hydrogen evolution measurements show that none of the coatings fulfill the requirement of a hydrogen evolution rate of 0,01 ml/(cm²day), as stated in [40], because the ALD-coatings allow for fluids to reach the magnesium surface. However, there are more factors influencing the biocompatibility of the coatings. As seen in the SEM-photos in Figure 4.1, the scratches from the mechanical polishing are clearly present in all images, indicating that the coatings are conformal. As an implant surface will be tailored to induce tissue growth, a protective coating should, therefore, follow the surface morphology - which the Zirconia-, Hafnia, and Titania-coatings did.

5.5 Suggestions for improving corrosion performance of ALD-coatings

The ALD-coatings investigated in this thesis are not sufficient for biomedical use. However, there are more ways of tuning the ALD-coatings than what has been explored in this thesis. For instance could combining coatings, as was done in [59], be a good alternative. Marin et al. [59] investigated AZ31-samples with ALD-coatings of TiO_2 , Al_2O_3 , and alternating coatings of $\text{Al}_2\text{O}_3/\text{TiO}_2$, and $\text{Al}_2\text{O}_3/\text{TiO}_2/\text{Al}_2\text{O}_3/\text{TiO}_2$. The thickness of each coating was 100nm in total. Polarisation curves were performed in 0.05M NaCl at room temperature, whereas the bare sample had a current density of $10^{-4}\text{A}/\text{cm}^2$. The TiO_2 -coating and Al_2O_3 -coating lowered the current density by two decades to about $10^{-6}\text{A}/\text{cm}^2$. The two alternating coatings, on the other hand, both lowered the corrosion current density to about $10^{-8}\text{A}/\text{cm}^2$. This is interesting, as there was a gap in magnitude of two decades for coatings with the same thickness. Hence, combining coatings were shown to have a sealing effect. The hypothesis of this sealing effect in [59] was that nucleation of one oxide would cover the defects of the other. Therefore could the challenge with nanometer gaps found in pure ALD-coatings be overcome by combining coatings.

5.6 Evaluation of experimental work

The human body's environment was, in the experiments conducted in this thesis, represented by SBF. Nevertheless, a human body has a temperature of about 37°C , but the experiments were run in room temperature. However, in a study by Wagener & Virtanen [85], they investigated how electrochemical measurements of pure magnesium in SBF acted at 37°C compared to room temperature. Their findings revealed that the temperature rise had minimal impact on the results. It is, therefore, believed that if the experiments in this thesis were conducted at 37°C , similar results to what already obtained, would be found.

The equivalent circuit (EC) that was used for simulating the EIS-spectra was chosen based on what had been used in literature with similar cases. However, what impact the choice of EC had on the results, was not investigated in this thesis. In order to verify the EIS-fitting results, such an investigation should be made.

6 Conclusion

In this master thesis, the performance of ALD-coatings on magnesium alloy AZ31 was investigated. This was done for the purpose of improving the corrosion resistance of magnesium alloys for use in biomedical implants. Zirconia-, Hafnia-, and Titania-coatings were deposited on magnesium alloy AZ31 substrates and was evaluated through potentiodynamic polarisation experiments, electrochemical impedance spectroscopy, and hydrogen evolution measurements. All results showed that ZrO_2 -, HfO_2 - and TiO_2 -coatings prepared by ALD improved the corrosion resistance of magnesium alloy AZ31 in SBF. However, their resistance was limited due to nanometer-gaps in the coatings. Moreover, if the AZ31 alloy is to be used for biomedical implants, the protection provided by neither one of these ALD-coatings is sufficient.

Yet, coatings prepared by ALD are highly conformal, which is an important property considering biomedical devices. Also, the protective properties are essentially the same for coatings prepared by ALD with thicknesses at nm-scale, compared to coatings prepared by other coating techniques with thicknesses at μm -scale. It is therefore suggested for further work to investigate combinations of different materials in the ALD-coating, where it is possible to make up for the defects present in the single-material coatings.

References

- [1] G. Eddy Jai Poinern, S. Brundavanam, and D. Fawcett, “Biomedical Magnesium Alloys: A Review of Material Properties, Surface Modifications and Potential as a Biodegradable Orthopaedic Implant,” *American Journal of Biomedical Engineering*, vol. 2, no. 6, pp. 218–240, 2013.
- [2] H. C. Knoops, S. E. Potts, A. A. Bol, and W. M. Kessels, “Atomic layer deposition,” in *Handbook of Crystal Growth: Thin Films and Epitaxy: Second Edition*, vol. 3, pp. 1101–1134, Amsterdam: Elsevier B.V., 2014.
- [3] P. Pedferri, “Evans diagrams,” in *Corrosion Science and Engineering*, pp. 103–118, Cham: Springer International Publishing, 2018.
- [4] M. Peron, J. Torgersen, and F. Berto, “Mg and its alloys for biomedical applications: Exploring corrosion and its interplay with mechanical failure,” *Metals*, vol. 7, no. 7, 2017.
- [5] M. Gupta and S. N. M. Ling, *Magnesium, magnesium alloys, and magnesium composites*. Hoboken: John Wiley & Sons, 2011.
- [6] P. H. Long, “Medical devices in orthopedic applications,” *Toxicologic Pathology*, vol. 36, no. 1, pp. 85–91, 2008.
- [7] M. Long and H. Rack, “Titanium alloys in total joint replacement—a materials science perspective,” *Biomaterials*, vol. 19, no. 18, pp. 1621 – 1639, 1998.
- [8] T. B. Matias, G. H. Asato, B. T. Ramasco, W. J. Botta, C. S. Kiminami, and C. Bolfarini, “Processing and characterization of amorphous magnesium based alloy for application in biomedical implants,” *Journal of Materials Research and Technology*, vol. 3, no. 3, pp. 203–209, 2014.
- [9] S. Dorozhkin, “Surface modification of magnesium and its biodegradable alloys by calcium orthophosphate coatings to improve corrosion resistance and biocompatibility,” in *Surface Modification of Magnesium and its Alloys for Biomedical Applications*, pp. 151 – 191, Sawston: Woodhead Publishing, 2015.
- [10] J. Wolff, *The Law of Bone Remodelling*. Berlin/Heidelberg: Springer, 1986.
- [11] G. Manivasagam and S. Suwas, “Biodegradable mg and mg based alloys for biomedical implants,” *Materials Science and Technology*, vol. 30, no. 5, pp. 515–520, 2014.

-
- [12] N. Li and Y. Zheng, "Novel magnesium alloys developed for biomedical application: A review," *Journal of Materials Science & Technology*, vol. 29, no. 6, pp. 489–502, 2013.
- [13] M. Moravej and D. Mantovani, "Biodegradable metals for cardiovascular stent application: Interests and new opportunities," *International Journal of Molecular Sciences*, vol. 12, no. 7, pp. 4250–4270, 2011.
- [14] L. Yang and L.-M. Zhang, "Chemical structural and chain conformational characterization of some bioactive polysaccharides isolated from natural sources," *Carbohydrate Polymers*, vol. 76, no. 3, pp. 349–361, 2009.
- [15] T. Sato, G. Chen, T. Ushida, T. Ishii, N. Ochiai, T. Tateishi, and J. Tanaka, "Evaluation of plla-collagen hybrid sponge as a scaffold for cartilage tissue engineering," *Materials Science & Engineering C*, vol. 24, no. 3, pp. 365–372, 2004.
- [16] V. Sinha and R. Kumria, "Polysaccharides in colon-specific drug delivery," *International Journal of Pharmaceutics*, vol. 224, no. 1, pp. 19–38, 2001.
- [17] J. M. Kanczler, P. J. Ginty, J. J. Barry, N. M. Clarke, S. M. Howdle, K. M. Shakesheff, and R. O. Oreffo, "The effect of mesenchymal populations and vascular endothelial growth factor delivered from biodegradable polymer scaffolds on bone formation," *Biomaterials*, vol. 29, no. 12, pp. 1892–1900, 2008.
- [18] Y. Dong and S.-S. Feng, "Methoxy poly(ethylene glycol)-poly(lactide) (mpep-pla) nanoparticles for controlled delivery of anticancer drugs," *Biomaterials*, vol. 25, no. 14, pp. 2843–2849, 2004.
- [19] L. Rimondini, N. Nicoli-Aldini, M. Fini, G. Guzzardella, M. Tschon, and R. Giardino, "In vivo experimental study on bone regeneration in critical bone defects using an injectable biodegradable pla/pgs copolymer," *Oral Surgery, Oral Medicine, Oral Pathology, Oral Radiology and Endodontology*, vol. 99, no. 2, pp. 148–154, 2005.
- [20] S. Ramakrishna, J. Mayer, E. Wintermantel, and K. W. Leong, "Biomedical applications of polymer-composite materials: a review," *Composites Science and Technology*, vol. 61, no. 9, pp. 1189–1224, 2001.
- [21] Y. Zheng, X. Gu, and F. Witte, "Biodegradable metals," *Materials Science & Engineering R*, vol. 77, pp. 1–34, 2014.

-
- [22] R. Singh Raman, S. Jafari, and S. E. Harandi, "Corrosion fatigue fracture of magnesium alloys in bioimplant applications: A review," *Engineering Fracture Mechanics*, vol. 137, pp. 97–108, 2015.
- [23] M. P. Staiger, A. M. Pietak, J. Huadmai, and G. Dias, "Magnesium and its alloys as orthopedic biomaterials: A review," *Biomaterials*, vol. 27, no. 9, pp. 1728–1734, 2006.
- [24] A. Hanzi, A. Sologubenko, and P. Uggowitzer, "Design strategy for new biodegradable mg-y-zn alloys for medical applications," *International Journal of Materials Research (Zeitschrift fur Metallkunde)*, vol. 100, no. 8, pp. 1127–1236, 2009.
- [25] E. Zhang, "Phosphate treatment of magnesium alloy implants for biomedical applications," in *Surface Modification of Magnesium and its Alloys for Biomedical Applications* (T. S. N. S. Narayanan, I.-S. Park, and M.-H. Lee, eds.), ch. 2, pp. 23–57, Elsevier Ltd., volume ii: ed., 2015.
- [26] T. S. Sankara Narayanan, I. S. Park, and M. H. Lee, "Strategies to improve the corrosion resistance of microarc oxidation (MAO) coated magnesium alloys for degradable implants: Prospects and challenges," *Progress in Materials Science*, vol. 60, no. 1, pp. 1–71, 2013.
- [27] S. Agarwal, J. Curtin, B. Duffy, and S. Jaiswal, "Biodegradable magnesium alloys for orthopaedic applications: A review on corrosion, biocompatibility and surface modifications," *Materials Science and Engineering C*, vol. 68, pp. 948–963, 2016.
- [28] H. Hornberger, S. Virtanen, and A. R. Boccaccini, "Biomedical coatings on magnesium alloys - A review," *Acta Biomaterialia*, vol. 8, no. 7, pp. 2442–2455, 2012.
- [29] C. Blawert, S. P. Sah, N. Scharnagl, and M. B. Kannan, "Plasma electrolytic oxidation/micro-arc oxidation of magnesium and its alloys," in *Surface Modification of Magnesium and its Alloys for Biomedical Applications* (T. S. N. S. Narayanan, I.-S. Park, and M.-H. Lee, eds.), ch. 8, pp. 193–234, Elsevier Ltd., volume ii: ed., 2015.
- [30] C. Piconi and G. Maccauro, "Review: Zirconia as a ceramic biomaterial," *Comprehensive Biomaterials*, vol. 20, pp. 1–25, 1997.

-
- [31] J. Li, X. Zhang, X. He, R. Hang, X. Huang, and B. Tang, "Preparation, biocompatibility and wear resistance of microstructured Zr and ZrO₂ alloyed layers on 316L stainless steel," *Materials Letters*, vol. 203, pp. 24–27, 2017.
- [32] T. Kääriäinen, D. Cameron, M.-L. Kääriäinen, and A. Sherman, *Atomic layer deposition: principles, characteristics, and nanotechnology applications*. John Wiley & Sons, 2013.
- [33] A. Markowska-Szczupak, K. Ulfig, and A. W. Morawski, "The application of titanium dioxide for deactivation of bioparticulates: An overview," *Catalysis Today*, vol. 169, no. 1, pp. 249–257, 2011.
- [34] K. Chen, J. Dai, and X. Zhang, "Improvement of corrosion resistance of magnesium alloys for biomedical applications," *Corrosion Reviews*, vol. 33, no. 3-4, pp. 101–117, 2015.
- [35] M. B. Kannan, "Biodegradable polymeric coatings for surface modification of magnesium-based biomaterials," in *Surface Modification of Magnesium and its Alloys for Biomedical Applications* (T. S. N. S. Narayanan, I.-S. Park, and M.-H. Lee, eds.), ch. 13, pp. 355–376, Elsevier Ltd., volume ii: ed., 2015.
- [36] N. Kirkland, J. Lespagnol, N. Birbilis, and M. Staiger, "A survey of bio-corrosion rates of magnesium alloys," *Corrosion Science*, vol. 52, no. 2, pp. 287 – 291, 2010.
- [37] R. W. Revie, *Uhlig's Corrosion Handbook (3rd Edition)*. New York: John Wiley & Sons, 2011.
- [38] C. Vargel, "Galvanic corrosion," in *Corrosion of Aluminium*, Amsterdam: Elsevier, 2004.
- [39] R. Ambat, N. N. Aung, and W. Zhou, "Evaluation of microstructural effects on corrosion behaviour of az91d magnesium alloy," *Corrosion Science*, vol. 42, no. 8, pp. 1433 – 1455, 2000.
- [40] G. Song, "Control of biodegradation of biocompatible magnesium alloys," *Corrosion Science*, vol. 49, pp. 1696–1701, apr 2007.
- [41] M. Razavi, M. Fathi, O. Savabi, D. Vashaei, and L. Tayebi, "In vitro study of nanostructured diopside coating on mg alloy orthopedic implants," *Materials Science & Engineering C*, vol. 41, no. 3, pp. 168–177, 2014.

-
- [42] S. Lynch, "Hydrogen embrittlement phenomena and mechanisms," *Corrosion Reviews*, vol. 30, no. 3, pp. 105–123, 2012.
- [43] S. Jafari, S. Harandi, and R. Singh Raman, "A review of stress-corrosion cracking and corrosion fatigue of magnesium alloys for biodegradable implant applications," *JOM*, vol. 67, no. 5, pp. 1143–1153, 2015.
- [44] F. Witte, V. Kaese, H. Haferkamp, E. Switzer, A. Meyer-Lindenberg, C. Wirth, and H. Windhagen, "In vivo corrosion of four magnesium alloys and the associated bone response," *Biomaterials*, vol. 26, no. 17, pp. 3557–3563, 2005.
- [45] M. O. Pekguleryuz, K. U. Kainer, and A. A. Kaya, *Fundamentals of magnesium alloy metallurgy*. Philadelphia: Woodhead Publishing, 2013.
- [46] D. Persaud-Sharma and A. McGoron, "Biodegradable Magnesium Alloys: A Review of Material Development and Applications," *Journal of Biomimetics, Biomaterials and Tissue Engineering*, vol. 12, pp. 25–39, feb 2012.
- [47] J. E. Hillis and R. W. Murray, "Finishing alternatives for high purity magnesium alloys," in *SDCE 14 th International Die Casting Congress and Exposition*, p. 1987, 1987.
- [48] F. Witte, N. Hort, C. Vogt, S. Cohen, K. U. Kainer, R. Willumeit, and F. Feyerabend, "Degradable biomaterials based on magnesium corrosion," *Current Opinion in Solid State & Materials Science*, vol. 12, no. 5, pp. 63–72, 2008.
- [49] H. A. Robinson and P. F. George, "Effect of alloying and impurity elements in magnesium alloy cast anodes," *CORROSION*, vol. 10, no. 6, pp. 182–188, 1954.
- [50] Q. Wang and M. Zhang, *Cold-spray coatings on magnesium and its alloys*, vol. 2. Elsevier Ltd, 2015.
- [51] P. R. Chalker, "Photochemical atomic layer deposition and etching," *Surface and Coatings Technology*, vol. 291, pp. 258–263, 2016.
- [52] O. Graniel, M. Weber, S. Balme, P. Miele, and M. Bechelany, "Atomic layer deposition for biosensing applications," *Biosensors and Bioelectronics*, vol. 122, no. July, pp. 147–159, 2018.

-
- [53] T. F. da Conceição and N. Scharnagl, “Fluoride conversion coatings for magnesium and its alloys for the biological environment,” *Surface Modification of Magnesium and Its Alloys for Biomedical Applications*, vol. 2, pp. 3–21, 2015.
- [54] R. M. Pilliar, “Sol-gel surface modification of biomaterials,” in *Surface Coating and Modification of Metallic Biomaterials* (C. Wen, ed.), no. 1, ch. 6, pp. 185–217, Elsevier Ltd, 2015.
- [55] H. R. Bakhsheshi-Rad, E. Hamzah, G. J. Dias, S. N. Saud, F. Yaghoubidoust, and Z. Hadisi, “Fabrication and characterisation of novel ZnO/MWCNT duplex coating deposited on Mg alloy by PVD coupled with dip-coating techniques,” *Journal of Alloys and Compounds*, vol. 728, pp. 159–168, 2017.
- [56] M. Leskela, E. Salmi, and M. Ritala, “Atomic layer deposited protective layers,” *Materials science forum*, vol. 879, 2016.
- [57] Y. Li, H. Li, Q. Xiong, X. Wu, J. Zhou, J. Wu, X. Wu, and W. Qin, “Multipurpose surface functionalization on AZ31 magnesium alloys by atomic layer deposition: Tailoring the corrosion resistance and electrical performance,” *Nanoscale*, vol. 9, no. 25, pp. 8591–8599, 2017.
- [58] Z. Li, S. Wu, X. Yang, X. Liu, Q. Yang, Z. Cui, K. W. Yeung, Y. Zheng, and W. Yuan, “A combined coating strategy based on atomic layer deposition for enhancement of corrosion resistance of AZ31 magnesium alloy,” *Applied Surface Science*, vol. 434, pp. 1101–1111, 2017.
- [59] E. Marin, A. Lanzutti, L. Guzman, and L. Fedrizzi, “Chemical and electrochemical characterization of TiO₂/Al₂O₃ atomic layer depositions on AZ-31 magnesium alloy,” *Journal of Coatings Technology and Research*, vol. 9, no. 3, pp. 347–355, 2012.
- [60] Q. Yang, W. Yuan, X. Liu, Y. Zheng, Z. Cui, X. Yang, H. Pan, and S. Wu, “Atomic layer deposited ZrO₂ nanofilm on Mg-Sr alloy for enhanced corrosion resistance and biocompatibility,” *Acta Biomaterialia*, vol. 58, pp. 515–526, 2017.
- [61] P. C. Wang, Y. T. Shih, M. C. Lin, H. C. Lin, M. J. Chen, and K. M. Lin, “A study of atomic layer deposited LiAl_xO_y films on Mg-Li alloys,” *Thin Solid Films*, vol. 518, no. 24, pp. 7501–7504, 2010.

-
- [62] X. Liu, Q. Yang, Z. Li, W. Yuan, Y. Zheng, Z. Cui, X. Yang, K. W. Yeung, and S. Wu, "A combined coating strategy based on atomic layer deposition for enhancement of corrosion resistance of AZ31 magnesium alloy," *Applied Surface Science*, vol. 434, pp. 1101–1111, 2018.
- [63] T. Kääriäinen, D. Cameron, M.-L. Kääriäinen, and A. Sherman, "Atomic Layer Deposition : Principles, Characteristics, and Nanotechnology Applicatons," in *Atomic Layer Depositon - Principles, Characteristics, and Nanotechnonology Applications*, ch. Chapter 4., pp. 107–111, John Wiley & Sons, Incorporated, 2013.
- [64] J. Niinistö, M. Putkonen, L. Niinistö, S. L. Stoll, K. Kukli, T. Sajavaara, M. Ritalac, and M. Leskeläc, "Controlled growth of HfO₂ thin films by atomic layer deposition from cyclopentadienyl-type precursor and water," *Journal of Materials Chemistry*, no. 23, 2005.
- [65] D. Li, D. Wu, Z. Yang, Y. Zhou, S. Wang, X. Duan, D. Jia, Q. Zhu, and Y. Zhou, "Effects of in situ amorphous graphite coating on ablation resistance of sic fiber reinforced sibcn ceramics in an oxyacetylene flame," *Corrosion Science*, vol. 113, pp. 31 – 45, 2016.
- [66] M. D. Anderson, B. Aitchison, and D. C. Johnson, "Corrosion Resistance of Atomic Layer Deposition-Generated Amorphous Thin Films," *ACS Applied Materials and Interfaces*, vol. 8, no. 44, pp. 30644–30648, 2016.
- [67] E. E. Stansbury, *Fundamentals of electrochemical corrosion*. S.l.: ASM International, 1 ed., 2000.
- [68] P. Pedferri, "Kinetics of aqueous corrosion," in *Corrosion Science and Engineering*, pp. 73–102, Cham: Springer International Publishing, 2018.
- [69] H. Cesiulis, N. Tsyntaru, A. Ramanavicius, and G. Ragoisha, "The study of thin films by electrochemical impedance spectroscopy," in *Nanostructures and Thin Films for Multifunctional Applications: Technology, Properties and Devices*, pp. 3–42, Cham: Springer International Publishing, 2016.
- [70] V. Silva, "Impedance spectroscopy," in *Encyclopedia of Membranes*, pp. 1023–1025, Berlin, Heidelberg: Springer Berlin Heidelberg, 2016.
- [71] D. Landolt, *Corrosion and surface chemistry of metals*. Lausanne: EPFL press, 2007.

-
- [72] G. Song, A. Atrens, and D. StJohn, “An hydrogen evolution method for the estimation of the corrosion rate of magnesium alloys,” in *Essential Readings in Magnesium Technology*, pp. 565–572, Cham: Springer International Publishing, 2016.
- [73] I. Polmear, “5 - magnesium alloys,” in *Light Alloys (Fourth Edition)* (I. Polmear, ed.), pp. 237 – 297, Oxford: Butterworth-Heinemann, fourth edition ed., 2005.
- [74] T. Kokubo and H. Takadama, “How useful is sbf in predicting in vivo bone bioactivity?,” *Biomaterials*, vol. 27, no. 15, pp. 2907–2915, 2006.
- [75] G. Song, A. Atrens, and D. Suohn, “An hydrogen evolution method for the estimation of the corrosion rate of magnesium alloys,” in *Essential Readings in Magnesium Technology*, vol. 9781118858943, pp. 565–572, Wiley Blackwell, 2014.
- [76] T. S. Lim, H. S. Ryu, and S.-H. Hong, “Electrochemical corrosion properties of ceo₂-containing coatings on az31 magnesium alloys prepared by plasma electrolytic oxidation,” *Corrosion Science*, vol. 62, pp. 104 – 111, 2012.
- [77] G. Song, A. Atrens, D. John, X. Wu, and J. Nairn, “The anodic dissolution of magnesium in chloride and sulphate solutions,” *Corrosion Science*, vol. 39, no. 10, pp. 1981 – 2004, 1997.
- [78] Y. Liu, Z. Yu, S. Zhou, and L. Wu, “Self-assembled monolayers on magnesium alloy surfaces from carboxylate ions,” *Applied Surface Science*, vol. 252, no. 10, pp. 3818 – 3827, 2006.
- [79] J. Zhao, X. Xie, and C. Zhang, “Effect of the graphene oxide additive on the corrosion resistance of the plasma electrolytic oxidation coating of the az31 magnesium alloy,” *Corrosion Science*, vol. 114, pp. 146 – 155, 2017.
- [80] Y. Xin, K. Huo, H. Tao, G. Tang, and P. K. Chu, “Influence of aggressive ions on the degradation behavior of biomedical magnesium alloy in physiological environment,” *Acta Biomaterialia*, vol. 4, no. 6, pp. 2008 – 2015, 2008.
- [81] X. Li, X. Liu, S. Wu, K. Yeung, Y. Zheng, and P. K. Chu, “Design of magnesium alloys with controllable degradation for biomedical implants: From bulk to surface,” *Acta Biomaterialia*, vol. 45, pp. 2 – 30, 2016.
- [82] L. Liu and M. Schlesinger, “Corrosion of magnesium and its alloys,” *Corrosion Science*, vol. 51, no. 8, pp. 1733 – 1737, 2009.

- [83] B. Díaz, E. Härkönen, J. Światowska, V. Maurice, A. Seyeux, P. Marcus, and M. Ritala, “Low-temperature atomic layer deposition of Al_2O_3 thin coatings for corrosion protection of steel: Surface and electrochemical analysis,” *Corrosion Science*, vol. 53, no. 6, pp. 2168 – 2175, 2011.
- [84] T. O. Kääriäinen, P. Maydannik, D. C. Cameron, K. Lahtinen, P. Johansson, and J. Kuusipalo, “Atomic layer deposition on polymer based flexible packaging materials: Growth characteristics and diffusion barrier properties,” *Thin Solid Films*, vol. 519, no. 10, pp. 3146 – 3154, 2011.
- [85] V. Wagener and S. Virtanen, “Influence of electrolyte composition (simulated body fluid vs. dulbecco’s modified eagle’s medium), temperature, and solution flow on the biocorrosion behavior of commercially pure mg,” *Corrosion*, vol. 73, pp. 1413–1422, 12 2017.

Appendices

A Specialization project

Norwegian University of Science and Technology

TMM4560 Specialization Project

Department of Mechanical and Industrial Engineering

December 12th , 2018

Surface coatings prepared by Atomic layer deposition to improve the biocorrosion resistance of magnesium alloys

Author

Maria Bjelland

Supervisor

Jan Torgersen



Preface

This specialization project was carried out during the autumn semester of 2018, at the Department of Mechanical and Industrial Engineering (MTP) at the Norwegian University of Science and Technology (NTNU).

I would like to acknowledge my supervisor Associate Professor Jan Torgersen and PhD Candidate Mirco Peron for their help and guidance during this project.

Abstract

The aim with this specialization project was to investigate through a literature study if ALD is a suited coating method for corrosion protection of magnesium alloys for clinical use. Various coating techniques for biocompatible corrosion protection of magnesium alloys was reviewed and evaluated for comparison to ALD. An overview of the current research on corrosion protection on magnesium by ALD was also established.

In conclusion, there is a large potential laying within ALD for corrosion protection of magnesium alloys for biomedical use. The coating-properties obtained by ALD are superior compared to coatings prepared by other coating techniques alone. The ALD process itself offer great composition control in addition to good adhesion, even at low temperatures, which is crucial for magnesium with its low melting point. Furthermore, there are so far little research on the specific field of ALD on magnesium in clinical applications, but the results available are promising.

Abbreviations

ALD	Atomic Layer Deposition
CSD	Chemical Solution Deposition
SBF	Simulated Body Fluid
CVD	Chemical Vapor Deposition
PBS	Phosphate Buffered Saline
PVD	Physical Vapor Deposition
PEO	Plasma Electrolytic Oxidation
MAO	Micro-Arc Oxidation
ALE	Atomic Layer Epitaxy
CMOS	Complementary Metal-Oxide-Semiconductor

Table of contents

Preface.....	i
Abstract	ii
Abbreviations	iii
Table of contents	iv
List of figures	v
List of tables	v
1 Introduction	1
1.1 Biomedical implants.....	1
1.2 Magnesium – a biodegradable material.....	2
1.3 Coating requirements	4
1.4 Objectives.....	4
1.5 Scope.....	4
2 Previous coating techniques used for corrosion protection of magnesium alloys for biomedical purposes.....	6
2.1 Conversion coatings	6
2.2 Coatings by sol-gel process.....	8
2.3 Chemical vapor deposition.....	10
2.4 Physical vapor deposition.....	11
2.5 Plasma electrolytic oxidation/ Micro-arc oxidation	13
3 Atomic Layer Deposition	15
3.1 The process.....	15
3.2 ALD for improving the corrosion properties of Magnesium	16
3.3 Potential biomaterial-candidates for ALD-coatings on magnesium.....	21
3.3.1 ZrO ₂	21
3.3.2 TiO ₂	21
3.3.3 HfO ₂	22
4 Results	23
4.1 Summarizing table on coatings prepared by techniques other than ALD	23
4.2 Summarizing table on coatings prepared by ALD	24
5 Discussion	26
5.1 ALD compared to other coating techniques.....	26
5.2 ALD for corrosion protection of magnesium	27
6 Conclusion and future work	28
References	29

List of figures

2.1	Electrochemical polarization curves of phosphate-treated and bare magnesium alloy samples in SBF (Zhang 2015).....	7
2.2	Polarization curves for A) Bare alloy, and treated samples anodized at B) 100V, C) 110, D) 120V, E) 130V and F) 140V (Jiang et al. 2017).....	8
2.3	Polarization tests results of bare and dip-coated AZ31 alloys with different heat treatment (Tang et al. 2013).....	9
2.4	Polarization test results for bare alloy and alloys coated with CVD at different deposition temperatures (G. Yang et al. 2018).....	10
2.5	PVD-processes suitable for magnesium and its alloys.....	11
2.6	Polarization test results from bare, ZnO and ZnO/MWCNT coated alloys (Bakhsheshi-Rad et al. 2017).....	12
2.7	Polarization test results of bare, and PEO-coated samples (Lin et al. 2014).....	14
3.1	Illustration of the four steps in ALD (Knoops et al. 2014).....	16
3.2	Hydrogen evolution rates (Liu et al. 2018).....	17
3.3	a) Cell viability and b) ALP viability (Q. Yang et al. 2017).....	19

List of tables

1.1	Mechanical properties of natural bone and different implant materials (Peron, Torgersen, and Berto 2017).....	1
3.1	Results from polarization tests (Liu et al. 2018).....	17
3.2	Results from polarization tests (Q. Yang et al. 2017).....	18
3.3	Results from polarization tests (Marin et al. 2012).....	19
3.4	Results from polarization tests (Y. Li et al. 2017).....	20
3.5	Results from polarization tests (P. C. Wang et al. 2010).....	20
4.1	Results from polarization tests conducted on coatings prepared by different coating techniques.....	23
4.2	Results from polarization tests conducted on coatings prepared by ALD.....	25

1 Introduction

1.1 Biomedical implants

For a material to be considered as a biomaterial, and hence can be used as an implant in the human body, there are several requirements that needs to be fulfilled. They must be biocompatible, i.e. cause no inflammatory, allergic or cancerous reactions (Matias et al. 2014). In addition to this, the material must be either bioinert or bioactive, meaning the implant does not interfere- or that the material interacts with the surrounding tissue respectively (Peron, Torgersen, and Berto 2017). If the material is not biodegradable, the materials chemical properties must also be considered in relation to corrosion, so no harmful particles are released (Dorozhkin 2015). Materials that fulfill these requirements are various polymers, metals, ceramics and composite materials (Peron, Torgersen, and Berto 2017).

So far only permanent implants have been used for load-bearing applications. Because of the excellent mechanical properties of metals, such as strength, toughness and long service life, these out-perform the other materials for permanent load-bearing implants. Due to the limitations of biocompatibility, the most commonly used metals are titanium and titanium alloys, stainless steels, and cobalt-chrome alloys (Matias et al. 2014; Dorozhkin 2015). Unfortunately, there are several limitations of these metallic implants. The mechanical properties of the current implants highly differ from the mechanical properties of natural bone, as seen in Table 1.1. Such a mismatch leads to the phenomena *stress shielding*. With stress shielding, the implant carries more load than the bone and the bone adapts to this change, thus changing its properties. The bone can either become thinner or more porous, both enhancing

Table 1.1 Mechanical properties of natural bone and different implant materials (Peron, Torgersen, and Berto 2017)

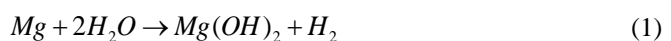
Properties	Natural bone	Stainless Steel	Ti Alloy	Co-Cr Alloy	Magnesium
<i>Density (g/cm³)</i>	1.7-2.0	7.9-8.1	4.4-4.5	8.3-9.2	1.74-2.0
<i>Elastic modulus (MPa)</i>	3-20	189-205	110-117	230	41-45
<i>Tensile strength (MPa)</i>	80-150	480-620	930-1140	900-1540	170-270
<i>Compressive yield strength (MPa)</i>	130-180	170-310	758-1117	450-1000	65-100
<i>Elongation at failure (%)</i>	1-7	30-40	8-15	30-45	6-20
<i>Fracture toughness (MPa m^{1/2})</i>	3-6	50-200	55-115	100	15-40

the risk of implant failure (Peron, Torgersen, and Berto 2017). Furthermore, toxic ions or particles can possibly be released from the implant due to corrosion and wear processes (Dorozhkin 2015). Hence, a patient will need a second surgery to remove the implant after healing. These surgeries can be complex and difficult, especially if tissues have grown around the implant.

1.2 Magnesium – a biodegradable material

Biodegradable implants can possibly overcome the challenges that comes with permanent implants. Being biodegradable, a material can corrode inside the body with biocompatible degradation products (Moravej and Mantovani 2011). A biodegradable implant must be able to give the support required for the damaged tissues until it has healed (Dorozhkin 2015). Magnesium has over the recent years gained attention for its biocompatibility and its outstanding properties for clinical use (Agarwal et al. 2016). With mechanical properties very similar to natural bone, the stress shielding phenomena is reduced (Matias et al. 2014). Magnesium can degrade naturally within the body, removing the need for second surgeries and hence reduce the healing time and possible complications that comes with post-surgeries (Dorozhkin 2015). Magnesium is also a vital part of the metabolism in the human body, crucial for many enzymes, and helps to stabilize DNA and RNA (Staiger et al. 2006). It is naturally found in the bone tissue and magnesium cations are the fourth most abundant cations in the human body (Dorozhkin 2015). Therefore, corrosion- or wear products from magnesium could possibly induce bone growth. On the other hand, too high levels of magnesium can give critical consequences, but this is rare as the body efficiently excretes excess magnesium in the urine (Staiger et al. 2006).

The biggest challenge that comes with magnesium as biodegradable implants is the poor corrosion resistance of the material. The healing time for a bone is about a year, and a bone implant should therefore keep its full integrity for the three first months before gradually degrading in both volume and strength (Zhang 2015). When in contact with or immersed in an aqueous solution, magnesium will react with water and corrode as according to Equation (1) (K. Chen, Dai, and Zhang 2015).



The anodic and cathodic partial reaction are given in equation (2) and (3) respectively.



As seen from the reactions, hydrogen gas bubbles will evolve, and the magnesium ions will react with the hydroxide and form magnesium hydroxide. This thin film has a low solubility in water, and therefore protects the metal from further corrosion. However, this film will react with the chloro-ions in the human body fluid and create magnesium chloride, as in Equation (4), which is highly soluble in water.



Thus, corrosion of magnesium will continue. Magnesium implants will hence suffer from early loss of mechanical properties, which can lead to implant failure before the surrounding tissue has time to heal (Zhang 2015). Another consequence from rapid corrosion, which has been reported by several in vivo studies, is the evolution of hydrogen gas bubbles around the implant (Zhang 2015). The maximum tolerable hydrogen evolution rate is 0.01 ml/(cm² day), which correspond to a corrosion rate of 0.02mm/year (Song 2007). The gas bubbles can potentially harm the healing process, cause necrosis in surrounding tissue (Sankara Narayanan, Park, and Lee 2013), and in worst case block the bloodstream of the patient (Peron, Torgersen, and Berto 2017). A fast degradation rate of magnesium can also give a rise in pH in the surrounding body fluid, which can affect the pH-dependent physiological reactions in the area, or even lead to an alkaline poisoning effect (Song 2007). It was reported by (Zhang 2015) that a rise in pH can lead to bone absorption in undesired regions due to an accelerated deposition of calcium phosphate. In the same article it was reported that a rise in pH may induce hemolysis. Likewise, a corrosive environment combined with an applied mechanical load, may also induce corrosion-assisted cracking phenomena (Peron, Torgersen, and Berto 2017).

To utilize the potential of magnesium as biodegradable implants, one evidently must improve the corrosion resistance. There are mainly two ways to improve the corrosion protection properties of magnesium; alloying, and coating. With alloying one can optimize the composition, microstructure and surface morphology (Agarwal et al. 2016). Alloying will increase the degradation resistance, but because alloying always gives the metal an inhomogeneous microstructure, bare magnesium alloys are prone to localized corrosion as pitting rather than uniform corrosion. Uniform corrosion is more desired as localized corrosion

can result in toxicity and early failure of the implant (Kannan 2015). With a coating on the other hand, one can prevent fluid entering the magnesium substrate and hence hinder corrosion.

1.3 Coating requirements

For biomedical applications, there are several requirements for a surface coating. Most importantly, the coating must non-toxic, thus not cause any harm to the surrounding environment (Zhang 2015). As the surface of the implant is where cells and new tissue will form, the coating must be biocompatible for these to adhere and grow. This is in regards of both surface morphology and coating composition. Additionally, as magnesium is biodegradable, so must the coating be. The aim with corrosion protection of magnesium implants is to slow down the initial degradation rate so tissues have time to heal, hence a coating will need to have a slower degradation rate than the magnesium itself. To be able to control and predict the degradation rate, uniform corrosion is desired, and it is therefore also advantageous if the coating has a uniform thickness. Being uniform, this also involve being pore free. Although pores may induce osseointegration (Blawert et al. 2015), the path for fluids to reach the surface are reduced when pores are present. Moreover, pores enhance the possibility of localized corrosion which further can introduce corrosion induced cracking phenomena.

1.4 Objectives

Recently, a coating technique called Atomic layer deposition (ALD) has gained attention for corrosion protection as it offers very thin, precise, conformal and pin-hole free coatings. In the ALD-process one can build coatings layer by layer and control the thickness on atom-scale. Unfortunately, there are still limited work available on this subject.

This specialization project will therefore aim, through a literature study, to investigate if ALD is a suited coating method for corrosion protection of magnesium alloys for clinical use. Additionally, the specialization project aims to establish an overview of what work has been done on the topic up until now. This is motivated by the possibility to, at a later stage, perform experiments which can lead to new knowledge in the field.

1.5 Scope

To conclude on whether ALD is a suitable method for corrosion protection of magnesium or not, a literature study has been conducted on common coating techniques for corrosion protection of magnesium, as well as ALD. This is presented in section 2 and 3. These sections

was prepared to create a proper basis for comparison, which is done in chapter 5. Additionally, in section 3, the review on ALD for corrosion protection is thorough to provide a current status on the topic up until now.

2 Previous coating techniques used for corrosion protection of magnesium alloys for biomedical purposes

As the properties of a coating depend on the application method, the coating technique should be carefully chosen. Several coating techniques have been investigated for improving the corrosion resistance of magnesium alloys for biomedical purposes, and this chapter gives an overview of the most common techniques.

2.1 Conversion coatings

When preparing conversion coatings, the substrate is immersed in an electrolyte where chemical reactions between the substrate and the content in the electrolyte form an insoluble film on the substrate surface (Packham 2011). The process is relatively short, varying from a few seconds to tens of seconds (Packham 2011). Conversion coatings can have thicknesses ranging from a few nanometers to several micrometers (Packham 2011), and the thickness is enhanced with increasing immersion time (Zhang 2015). The composition of the coating depends on several variables as substrate type, electrolyte, pH, temperature, and time and thus the process can be difficult to control and hence the specific chemistry of the coating (Packham 2011). The most common conversion coatings used to improve the corrosion resistance of magnesium for biomedical use are fluoride- and phosphate-based coatings.

Almost all work on phosphate treatment of magnesium alloys reports that the coating enhanced the corrosion properties (Zhang 2015). (Zhang 2015) presents results from polarization tests in simulated body fluid (SBF) of a phosphate treated magnesium alloy. The results, as seen in Figure 2.1, clearly indicate that the corrosion resistance is improved by the coating and is further improved by increasing immersion time (thickness).

Conversion coatings offers great adhesion to the substrate due to chemical bonds and an in-between layer between the substrate and the coating (X.-B. Chen et al. 2015). This was reported by for instance (Y. Chen et al. 2012), who reported that a phosphate conversion coating can be regarded as built up by two layers, where the inner layer is dense and amorphous, while the outer is porous consisting of crystals. Additionally, it was reported that the adhesion between the two layers was poorer than the adhesion between the lower layer on the substrate, which was suggested as a disadvantage. Another phenomenon that comes with the two-layer-coating

is that when a phosphating process is extended, the outer layer shifts to a rough brushite layer. The rough surface gives good corrosion properties, but may hinder cell adhesion (Zhang 2015).

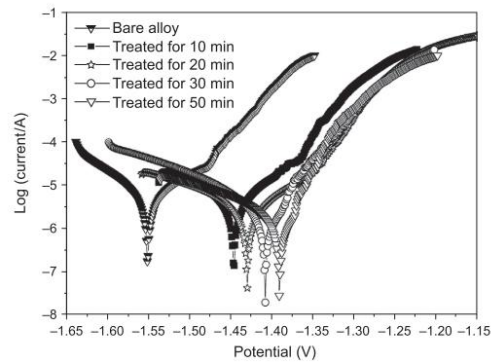


Figure 2.1 Electrochemical polarization curves of phosphate-treated and bare magnesium alloy samples in SBF (Zhang 2015).

Surface treatment by phosphate has already successfully been used on medical implants of Ti and its alloys, where a calcium-phosphate coating was deposited on the surface of the implants. The motivation was to avoid corrosion products in the body and to help the implant attach to the surrounding tissue. The benefits of the coating are possible due to phosphates good biocompatibility to bone tissue. (Zhang 2015)

The most studied fluoride conversion coating is MgF_2 , which in addition to improving the corrosion resistance, has been reported to have antibacterial properties and aid bone healing (da Conceição and Scharnagl 2015). However, (da Conceição and Scharnagl 2015) reported about poor long-term protection. This was assumed to be due to cracks and pores in the coating, and it was suggested that if a conversion coating should be used for corrosion protection of magnesium, a top coating should be applied.

When applying an external voltage to the conversion coating process, the process is called anodizing (Packham 2011). In a study by (Jiang et al. 2017), they investigated the degradation of AZ31 alloys with MgF_2 -coatings formed by anodizing. The coating thicknesses varied between $1\mu m$ to $14\mu m$, and the higher voltage applied the thicker. They observed that for voltages below 120 V in the anodization process, the coating surface was rough and non-uniform, while for voltages above 120 V the coating surface was relatively fine, porous and uniform. In agreement to what was described for conversion coatings by (Zhang 2015), they

also concluded that increased thickness corresponds to increased corrosion resistance. Noteworthy, the lowest current density was obtained in the second-thickest sample, yielding $8.533 \times 10^{-7} \text{ A/cm}^2$. The thickest sample measured a current density of $4.36 \times 10^{-6} \text{ A/cm}^2$, but had the lowest potential as seen in Figure 2.2.

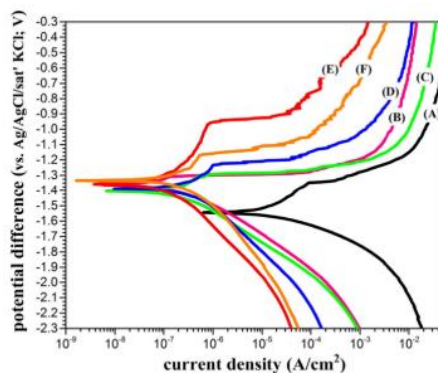


Figure 2.2 Polarization curves conducted in Hank's solution for A) Bare alloy, and treated samples anodized at B) 100V, C) 110, D) 120V, E) 130V and F) 140V (Jiang et al. 2017).

The polarization curves in the figure also revealed, on the anodic parts, kinks relatively close to the corrosion potential for the samples coated at and above 120V. This may indicate the onset of pitting corrosion on these samples, which is in correspondence with their reported porous surface. Hence, for long-term properties, anodizing will not give sufficiently protection without sealing the pores in the coating (Q. Wang and Zhang 2015).

2.2 Coatings by sol-gel process

The sol-gel process, also called chemical solution deposition (CSD), is a wet chemical method. The film is formed by colloidal suspension of either inorganic or metal organic precursors (Pilliar 2015). The process is simple, and the application areas are many, such as heat-sensitive materials and complex shapes (Hiromoto 2015). Because the process temperature is low, defects as phase transformations and changes in microstructures are avoided, and one can easily control the chemistry and structure of the coating accurately (Pilliar 2015). Sol-gel processing also results in good adhesion between the coating and the substrate (Asri et al. 2016). Nevertheless, the process often tends to form dots or heaps on the surface rather than a uniform coating (Hiromoto 2015), which is a disadvantage for corrosion protection. The sol-gel coatings also tend to crack upon drying (Pilliar 2015).

The sol-gel process can be carried out with different methods as for instance dip-coating, spin-coating, spray-coating and roll-coating. In dip-coating one simply dip the specimen in the solution, and the coating is applied. The thickness of the coating depends on number of dips, viscosity of the solution, and the dip rate (Augello and Liu 2015). The method is suited for thicker coatings, as it is hard to control the thickness of the coating. With spin-coating and roll-coating, better thickness control is achieved (Pilliar 2015). In spin coating, the solution is applied at the middle of the specimen, and the specimen is then spun to evenly distribute the solution on the surface. In roll-coating, the solution is fed to a wheel which rolls over the surface, and hence distributes the solution. The drawback of these two methods are that they are limited to flat specimens. Spray-coating can be applied to various shapes and is similar to dip-coating, and the method includes spraying the coating onto the substrate. Spray-coating can also provide a more uniform thickness than spin-coating.

(Tang et al. 2013) studied the corrosion properties of an AZ31 magnesium alloys coated with hydroxyapatite by sol-gel dip-coating. After dipping, the alloys were heated at 60°C for 30 minutes, before heat-treated at 200 °C and 400 °C for 30 minutes. The different specimens were immersed in SBF at 37°C to conduct polarization tests, and the results showed that the corrosion properties clearly were enhanced. The results also revealed that post-heat treatment greatly enhances the properties of the coating, as seen in Figure 2.3, by removing the water present in the coating and making the coating denser and more compact due to shrinkage. It was also reported that the adhesion was improved by post-heating.

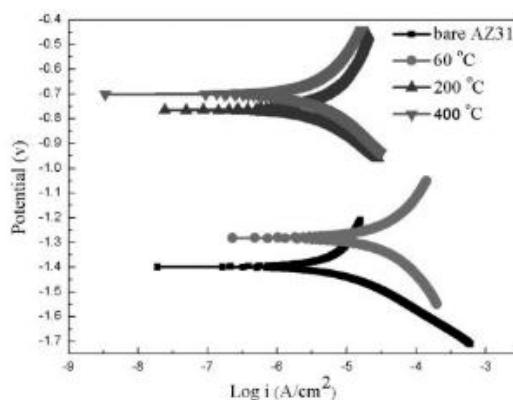


Figure 2.3 Polarization tests results of bare and dip-coated AZ31 alloys with different heat treatment (Tang et al. 2013).

2.3 Chemical vapor deposition

Chemical vapor deposition (CVD) is the collective name for a number of processes where a thin film is formed by chemical reactions between the substrate surface and the vapor. ALD, as discussed later, is a CVD-technique. The reaction happens on or nearby the substrate surface, and the substrate is normally pre-heated (Carlsson and Martin 2010). CVD offers great control of the deposition process, hence CVD-coatings in general has uniform thickness, and other properties can be tailored after need (Carlsson and Martin 2010).

In a recent study by (G. Yang et al. 2018), they deposited carbon nitride by one-step chemical vapor deposition (OS-CVD) on an AZ31B alloy. The process was conducted at three different temperatures; 400°C, 450°C and 500°C. The thickness of the all three coatings was about 4.69µm, and the films were uniform, dense and smooth. Immersion tests in phosphate-buffered saline (PBS) at 37°C for 180 hours revealed that the coated alloys surfaces remained intact without visible cracks or pits, and hydrogen evolution was low for all coated samples. Polarization tests in PBS at 37°C, as shown in Figure 2.4, showed that the sample coated at 500°C yielded best corrosion performance, but hemolysis testing showed that only the sample coated at 450°C was within the requirement of 5%.

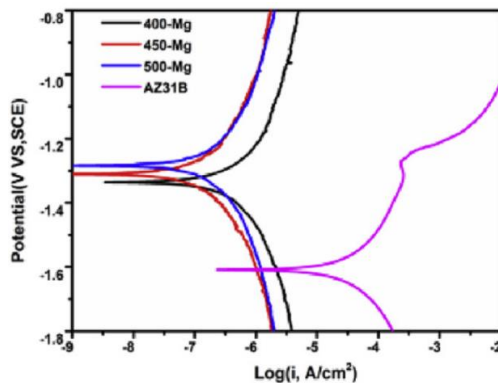


Figure 2.4 Polarization test results for bare alloy and alloys coated with CVD at different deposition temperatures (G. Yang et al. 2018).

For cell experiments and animal testing, they therefore continued with that sample. The coated alloy did not damage cells in the cell experiment and demonstrated good biocompatibility. This was consistent with the in vivo testing with rabbits, where lungs, kidney, liver and heart were investigated after one month. No inflammation, bleeding, necrosis or discoloration was

discovered for the coated alloy, while for the bare alloy some damage to the lungs were observed. The coated alloy also demonstrated good osseointegration.

Another study on coatings prepared by CVD was done by (Surmeneva et al. 2018), who coated AZ91, AZ31 and WE43 alloys with a 2 μm thick Parylene C-coating, a polymer with a dense structure and smooth hydrophobic surface. It was reported that the coating surfaces after deposition was uniform, smooth and more homogenous than the substrate surface. By polarization tests in Hank's solution it was proven that the coating is an effective corrosion inhibitor. More interestingly, in nanoindentation tests the Parylene C-coating showed an elastic behavior. This is advantageous for load-bearing implants, as the coating can follow the behavior of the implant without cracking and allowing fluids reaching the substrate surface.

2.4 Physical vapor deposition

Physical vapor depositions (PVD) main advantage is that the deposition can be done at low temperatures, that is temperatures well below the melting point of the substrate that is to be coated. This is especially an advantage with magnesium and magnesium alloys, as these materials are known as sensitive to temperature (Abela 2015).

To deposit a coating by PVD one evaporates a condensable material by very high temperature or kinetic energy, thereafter the vapor is transported by vacuum to a cold surface on the substrate. By surface diffusion, the vapor will form a thin solid film on the surface. Even though the deposition can occur at low temperatures, it is still challenging to use PVC on magnesium and its alloys due to control of deposition temperature and to secure sufficient adhesion at low temperatures (Abela 2015). Because of this, the only PVD processes that are suitable for magnesium and its alloys are the ones where the energy needed in the process are provided by plasma or high-energy flux, as condensable flux or ion beam (Abela 2015). These PVD-processes are summarized in Figure 2.5. In these processes there are no need for heating the substrate in advance.

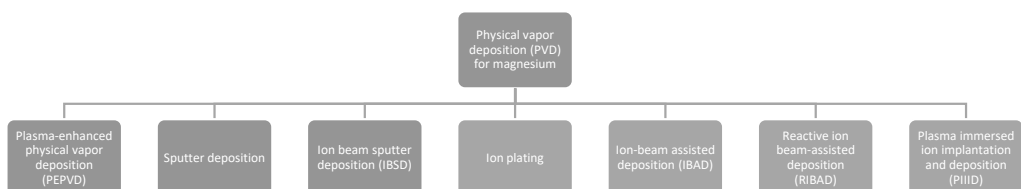


Figure 2.5 PVD-processes suitable for magnesium and its alloys

The main difference between the ion-assisted deposition techniques and plasma enhanced techniques is that in the first mentioned the energetic ion source and the condensable material flux is separated, allowing more control of each deposition parameter. This in turn improves the coating properties compared to plasma enhanced techniques, where the ion flux and condensable material flux comes from the same plasma source (Abela 2015).

In a study done by (Bakhsheshi-Rad et al. 2017), a Mg-0.8Ca-3Zn alloy was coated with a duplex coating consisting of ZnO and multi-walled carbon nanotubes (MWCNT), where ZnO was prepared by PVD and MWCNT by dip-coating. First mentioned was 1.1 μm thick, while second was 10.2 μm thick. As expected, polarization tests in SBF showed that the duplex coating performed better than the bare alloy and the alloy coated with only ZnO, as indicated in Figure 2.6.

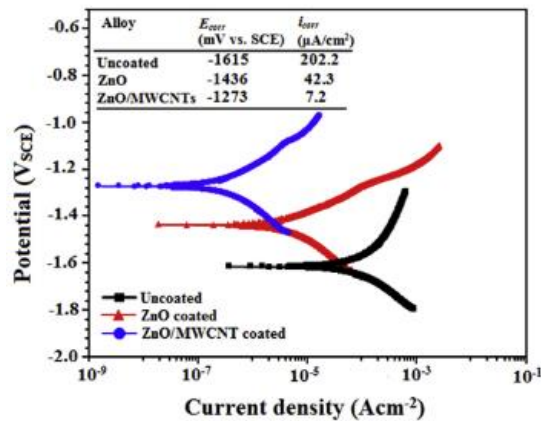


Figure 2.6 Polarization test results from bare, ZnO and ZnO/MWCNT coated alloys (Bakhsheshi-Rad et al. 2017).

More interestingly, after immersion for 10 days, both the ZnO coated alloy and the ZnO/MWCNT alloy experienced cracks and pits on the surface. However, the ZnO/MWCNT coated alloys experienced less corrosion damages and showed smaller corrosion rate than the ZnO-coated alloy. It was also reported that the ZnO/MWCNT coating showed great biocompatibility and favored osseointegration. These results indicate that coatings by PVD may not provide sufficient corrosion protection alone but need a top coating. This was also reported by (Abdal-Hay et al. 2014), who prepared a TiO (100nm) / PLA (1.8 μm) coating on alloy AM50 with PVD and dip-coating, where the PLA coating significantly improved the degradation properties in comparison to the TiO-coating alone.

2.5 Plasma electrolytic oxidation/ Micro-arc oxidation

Plasma electrolytic oxidation (PEO), also known as micro-arc oxidation (MAO) is a coating method that has been used in several industries for decades. When preparing a PEO-coating, the metal sample is immersed in an electrolyte. The metal sample works as an anode and working electrode, and usually the electrolyte container works as the counter electrode. High voltage is applied between the sample and the container, and the oxide layer on the metal is damaged as the dielectric breakdown voltage is exceeded and discharges occur. The coating material forms by local ionic transport from the electrolyte to the broken-down areas on the metal where a thicker oxide-layer is formed. The resulting coating is highly crystalline and thus is a hard coating with good resistance to wear. (Blawert et al. 2015)

Due to micro-discharges during the PEO-process, pores are often present in coatings prepared by PEO which is a major challenge as it allows for fluids to reach the substrate surface which initiate corrosion (Blawert et al. 2015). PEO-coatings therefore only provide moderate corrosion resistance (Narayanan, Park, and Lee 2015). Sealing coatings on top of PEO-coatings has been used to reduce the problem, and especially biocompatible and biodegradable polymers and co-polymers (PLA, PGA) has been mentioned as good candidates (Blawert et al. 2015). Although pores have been regarded as negative for the mechanical properties of the coating, it should be emphasized that for bone growth pores is advantageable, as new blood capillaries can grow into the graft (Blawert et al. 2015). The relationship between porosity and mechanical properties must therefore be thoroughly evaluated.

PEO-coatings have the advantage of growing both inwards and outwards of the metal specimen, which secures very good adhesion of these coatings. (Blawert et al. 2015) Micro-structure, surface morphology and composition of the coatings will influence the coating properties, and these matters can be modified for desired properties. The composition of the coating depends highly on the chosen electrolyte, as demonstrated by (Lin et al. 2014), who coated a ZK60 magnesium alloy by PEO to form a thin phosphate-based film containing strontium. Two different coatings were tested, one without strontium and one containing strontium, with thickness 10 and 20 μm respectively. The electrolytes used for preparation were the same except some $\text{Sr}(\text{OH})_2$ was added in one of them. The motivation for adding strontium, was a hypothesis that the element would improve biocompatibility. This was proven by cell tests and measuring ALP. By inspecting the coatings, it was clear that both coatings were porous and had micro-

holes, but both coatings enhanced the corrosion resistance (measured in Hank's solution at 37°C) as shown in Figure 2.7.

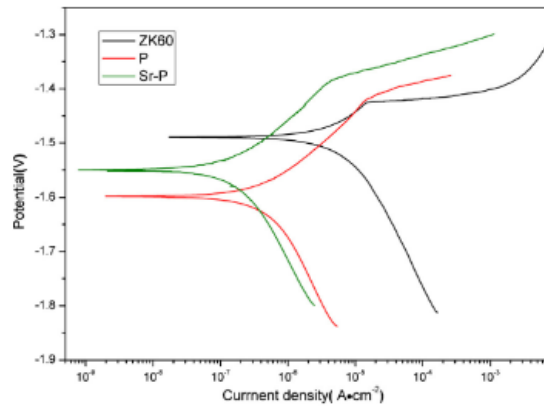


Figure 2.7 Polarization test results of bare, and PEO-coated samples (Lin et al. 2014). *P* denotes the sample prepared in an electrolyte without strontium, and *Sr-P* denotes the sample prepared in the electrolyte with strontium.

Nevertheless, for the coating with strontium, no damage of the coating was detected after 50 days of immersion, while for the bare sample and the other coated sample, severe local corrosion had occurred.

3 Atomic Layer Deposition

Atomic layer deposition is a coating technique based on chemical vapor deposition (CVD) which prepare thin films with high conformality and offers thickness control on atomic level (Graniel et al. 2018). The resulting film is dense and pin-hole free. The technique has its origin from the 1970's where it was developed with purpose to deposit ZnS for electroluminescent displays (Graniel et al. 2018). The technique was at the time named atomic layer epitaxy (ALE), as the films were going to be built up by crystalline or polycrystalline materials (Knoops et al. 2014). Later the technique was introduced to other application areas such as photovoltaics, catalysis and semiconductors (Puurunen 2014). Stated by (Knoops et al. 2014) was the ALE-technique especially used for forming *highly insulating oxide films to be used as low-leakage high-k dielectrics in complementary metal-oxide-semiconductor (CMOS) transistors and dynamic random access memory (DRAM) devices*. Applications like these have been the main reason for research on the technique which from the 1980's has been referred to as ALD (Graniel et al. 2018). Today ALD is used in applications as high-*k* gate dielectrics, resistive memory, and corrosion protection (Provine et al. 2016). In the semiconducting industry ALD is now popular due to its ability to be repeated, and control of composition and thickness (Chalker 2016). For biomedical purposes, ALD has gained a lot of attention over the last years as it offers compatibility on the nano-scale with the components involved, control of material composition regarding biocompatibility, and control of chemical reactivity (Graniel et al. 2018).

3.1 The process

In ALD, the thin films are built up by chemical reactions between two gaseous or vapor-phase precursors. One of the precursors is the main precursor and the other is the co-reactant, also called the second precursor (Chalker 2016). The dosing of the precursors is alternating and separated (Knoops et al. 2014). The process is self-limiting due to a limited number of reactive groups on the surface, and because the reactions are surface-reactions and not gas-reactions, ALD provides superior film uniformity (Chalker 2016). In (Knoops et al. 2014) and (Graniel et al. 2018), the process is divided into four steps, as illustrated in Figure 3.1:

- (1) The main precursor is applied into the reactor chamber and is left until it has reacted with the available surface groups on the specimen. The precursor is often an inorganic coordination compound (a metal centre with ligands).

- (2) The excess precursor is thereafter pumped or purged out of the reactor chamber by an inert gas, usually N₂ or Ar. This is an important step when the cycle is repeated to make sure that the precursor and co-reactant does not react with each other in the gas phase.
- (3) The second precursor, often a small molecule, is introduced when the system is cleared, which reacts with the molecules on the surface from the first precursor.
- (4) The system is then again purged or pumped.

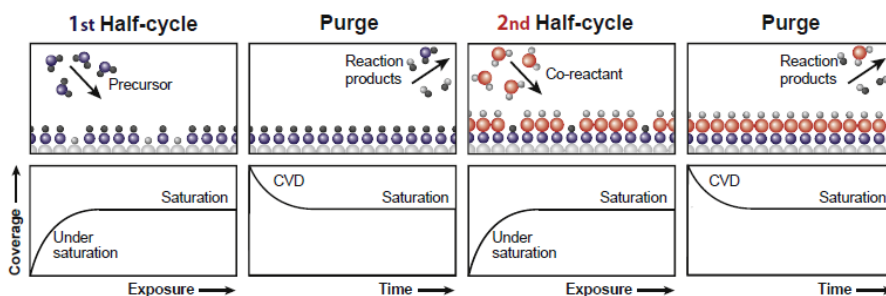


Figure 3.1 Illustration of the four steps in ALD (Knoops et al. 2014).

This process, or cycle, deposits a monolayer on substrate surface. To increase the thickness of the film, the cycle is repeated. For the process to work, it is crucial that the precursor and the co-reactant do not react with each other, themselves nor the reaction products. This is to make sure that the reactions happen on the substrate surface, and that the process will be self-limiting in the sense that when the surface is saturated, the deposition stops (Knoops et al. 2014).

3.2 ALD for improving the corrosion properties of Magnesium

Even though there is a growing interest for using ALD for corrosion protection of magnesium, there so far are few papers on the field. This section will give an overview.

(Liu et al. 2018) successfully coated an AZ31 alloy with a hybrid coating consisting of ZrO₂ and PLGA. The motivation for this combination was that ZrO₂ has outstanding biocompatibility and good corrosion resistance but is often damaged during the fabrication process. Hence, PLGA, a biocompatible and biodegradable polymer, was added as top-coat to make up for these potential defects. The ZrO₂-coating was deposited with ALD, where one sample was coated by 25 cycles and another with 100 cycles. The film deposition rate was reported to be around 0.117nm/cycle. The PLGA top coating was prepared through spin coating. The hybrid coating was shown to have good adhesion to the substrate and a Young's modulus not far from natural

bone. Corrosion tests were conducted on two samples while immersed in 0.9% NaCl at 37°C. Results from the dynamic potential polarization tests are shown in Table 3.1:

Table 3.1 Results from polarization tests (Liu et al. 2018)

	Untreated	ZrO ₂ (25 cycles)	PLGA/ZrO ₂ (25 cycles)	ZrO ₂ (100 cycles)	PLGA/ZrO ₂ (100 cycles)
E_{corr} (V _{SCE})	-1.557	-1.523	-1.518	-1.462	-1.452
i_{corr} (A/cm ²)	5.124×10^{-4}	1.546×10^{-5}	1.038×10^{-6}	2.775×10^{-7}	4.902×10^{-9}

Overall it was shown by dynamic potential polarization- and EIS-tests that coatings of both of ZrO₂ and a hybrid coating with PLGA improved the corrosion resistance of the magnesium alloy. Nevertheless, it was shown that the thickness of the ZrO₂-layer greatly influences the long-term properties. The hydrogen evolution tests revealed that the 25 cycle ZrO₂ coating accelerated the corrosion process after 72 hours of submersion, while the 100 cycle ZrO₂ coating showed great corrosive properties the complete immersion time. This was due to galvanic corrosion between the coating and substrate, as there existed some nano gaps in the coating. The hydrogen evolution graph for 96 hours is given in Figure 3.2. A PLGA top-coat will help the fill the existing gaps in the coating, which in the figure can be seen to have been efficient for the 100 cycle ZrO₂, but for the 25 cycle ZrO₂ worsened the results after a period of 24 hours. The reason was identified to be due to the formation of a local acidic microenvironment as a consequence of swelling and hydrolysing of PLGA. This again led to the electrolyte reaching the substrate surface and accelerated the galvanic corrosion.

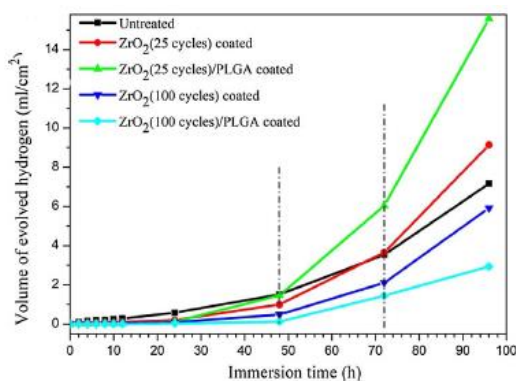


Figure 3.2 Hydrogen evolution rates (Liu et al. 2018)

In (Q. Yang et al. 2017) they also coated a magnesium alloy (Mg-Sr) with an ZrO₂ coating with the help of ALD. Corrosion tests were carried out with the samples immersed in SBF at 37°C for eight days. The results from the polarization tests are shown in Table 3.2.

Table 3.2 Results from polarization tests (Q. Yang et al. 2017)

	<i>Untreated</i>	<i>ZrO₂ 100 cyc.</i>	<i>ZrO₂ 200 cyc.</i>	<i>ZrO₂ 300 cyc.</i>	<i>ZrO₂ 400 cyc.</i>
$E_{corr} (V_{SCE})$	-1.928	-1.88	-1.83	-1.647	-1.75
$i_{corr} (A/cm^2)$	3.065×10^{-4}	1.536×10^{-4}	5.102×10^{-5}	1.318×10^{-5}	4.88×10^{-6}

Similar to (Liu et al. 2018), the results showed that the thicker the coating the better the protective properties. This was also supported by EIS tests. It was pointed out that it is not necessary that the thickness itself raises the corrosion resistance, but rather that the thickness makes up for other factors that influence the protective properties such as surface roughness and corrosion of zirconia itself. Results also showed that the thicker the coating, the less increase in pH. The problem with nano gaps, as discussed in (Liu et al. 2018), was also discussed here. When measuring the weight loss rates during the immersion time, the rates were continuously decreasing for the 100- and 200 cycle samples. For the 300- and 400-cycle samples, the weight loss rate decreased at first but then later increased. However, the rates were still lower than the 100- and 200-cycle samples. It was suggested that this may be due to corrosion products hindering corrosion at first, but that the electrolyte penetrates at a later stage.

(Q. Yang et al. 2017) also investigated the cytocompatibility with cells (MC3CT3 cell of mice) by a cell culture test. This was done with a bare sample and a sample coated with 400 cycles of ZrO₂ immersed in SBF. The cell viability was investigated by an MTT assay. Figure 3.3a) shows the cell viability with immersion time and 3.3b) demonstrates the alkaline phosphatase (ALP) levels. ALP is a measure of the osteogenic differentiation property, which is a crucial property for bone healing (Q. Yang et al. 2017).

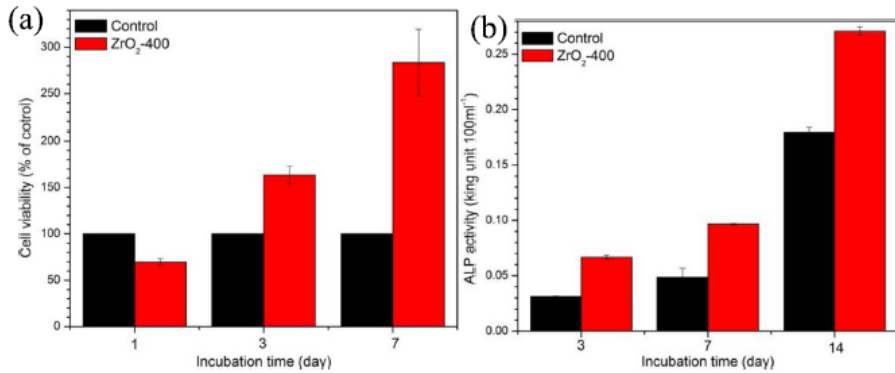


Figure 3.3 a) Cell viability and b) ALP viability (Q. Yang et al. 2017)

One can clearly see from the graphs that the coated samples performed better in regards of cytocompatibility, and it was concluded in the article that the coating will be beneficial for cell- and tissue growth.

(Marin et al. 2012) coated AZ31 alloys with both mono- and multilayers consisting of TiO₂ and Al₂O₃ to improve the corrosive properties of the alloy. The aim of the report was not to enhance biocorrosion properties and therefore the biocompatibility of the coatings was not emphasized. Four different samples were coated using ALD, one with a single layer of TiO₂, the second with a single layer of Al₂O₃, the third with Al₂O₃/TiO₂ bilayer and the fourth with a multilayer Al₂O₃/TiO₂/Al₂O₃/TiO₂. The samples were left rough to imitate ALD conditions in the industry. Because of the roughness, the thickness was rather difficult to measure, but was estimated to be 100-110 nm for all four coatings. When comparing SEM images from before and after deposition, one could in both cases still observe the rough surface indicating that the coatings were conformal. Corrosion tests was conducted in 0.05M NaCl at 20°C, and polarization tests showed that all coatings improved the corrosion properties compared to the bare alloy. The results are shown in Table 3.3.

Table 3.3 Results from polarization tests (Marin et al. 2012)

	Untreated	TiO ₂	Al ₂ O ₃	Al ₂ O ₃ /TiO ₂	Al ₂ O ₃ /TiO ₂ /Al ₂ O ₃ /TiO ₂
E_{corr} (V _{Ag/AgCl})	-1.48	-1.61	-1.46	-1.58	-1.57
i_{corr} (A/cm ²)	10 ⁻⁴	10 ⁻⁶	10 ⁻⁶	10 ⁻⁸	10 ⁻⁸

In the study done by (Y. Li et al. 2017), a AZ31 magnesium alloy was coated with a composite coating consisting of a PEO-layer and an aluminium doped zinc-oxide (AZO) film deposited by ALD (100 nm). As coatings prepared by PEO often has cracks and pinholes, the motivation for applying and ALD-coating on top was to fill these. The goal was to investigate both conductivity and corrosion properties of the coating, and results showed that both were enhanced with the composite coating. The PEO-coating was insulating, while the composite coating raised the conductivity to 25 S m^{-1} . Corrosion tests was carried out in a 3.5 wt% NaCl solution at room temperature, and results from the polarization tests are shown in Table 3.4.

Table 3.4 Results from polarization tests (Y. Li et al. 2017)

	<i>Untreated</i>	<i>PEO</i>	<i>PEO/AZO</i>
$E_{corr}(V_{SCE})$	-1.561	-1.343	-0.550
$i_{corr}(A/cm^2)$	3.16×10^{-4}	1.45×10^{-7}	1.36×10^{-6}

(P. C. Wang et al. 2010) studied atomic layer deposited LiAl_xO_y films with different thicknesses on an Mg-Li alloys. The motivation was not biomedical purposes, and hence the biomaterials was not chosen. By SEM-inspection it could be seen that the film was successfully deposited and conformal. Corrosion tests was also in this article carried out in a 3.5 wt% NaCl electrolyte. In agreement with the discussed articles, (P. C. Wang et al. 2010) concluded with that an ALD coating could significantly increase the corrosion resistance of an Mg alloy, and the thicker the coating the better. The polarization test results are shown in Table 3.5.

Table 3.5 Results from polarization tests. These values have been read of the graph in the article (P. C. Wang et al. 2010) by the author of this project.

	<i>Untreated</i>	<i>LiAl_xO_y (65 nm)</i>	<i>LiAl_xO_y (130 nm)</i>	<i>LiAl_xO_y (200 nm)</i>
$E_{corr}(V_{SCE})$	-1.46	-1.37	-1.18	-1.08
$i_{corr}(A/cm^2)$	2×10^{-3}	5×10^{-4}	3×10^{-4}	10^{-4}

3.3 Potential biomaterial-candidates for ALD-coatings on magnesium

In this section, three potential candidates for ALD-coatings to improve the biocorrosion of magnesium alloys are evaluated. These three are chosen based on the literature study and availability for further investigation.

3.3.1 ZrO_2

Due to Zirconium's excellent biocompatibility and mechanical properties, has it been used for a various range of prosthetic devices (Sollazzo et al. 2008). When exposed to oxygen, ZrO_2 is formed, which is a very stable oxide shown to favour osseointegration and cytocompatibility (J. Li et al. 2017). Its brilliant chemical stability and resistance to wear makes it suitable for corrosion protection purposes (Piconi and Maccauro 1997).

As discussed in section 3.2, ZrO_2 -coatings prepared by ALD have been already been prepared on magnesium alloys for corrosion protection, and the results were promising. However, as pointed out by (Liu et al. 2018) these films can crack during formation. They suggested that this could be made up for by increasing the number of cycles, alternatively a top coat. (Q. Yang et al. 2017) also demonstrated that increasing the thickness enhanced the properties. Hence, ZrO_2 is a suitable candidate for the purpose of improving biocorrosion resistance on magnesium, but further investigation is necessary.

3.3.2 TiO_2

TiO_2 is a common ALD material for corrosion protection purposes (Salmi 2015). TiO_2 is a super-hydrophilic coating with good chemical and physical stability (Kääriäinen et al. 2013). It is non-toxic for the human body and has anti-bacterial properties (Markowska-Szczupak, Ulfig, and Morawski 2011). It has been reported that when bioinert magnesium is coated with TiO_2 , the surface become bioactive and favours the formation of calcium phosphates (Hernández-Montes, Betancur-Henao, and Santa-Marín 2017).

It can be challenging to deposit TiO_2 due to poor adhesion and homogeneity caused by some deposition techniques. However, TiO_2 has already successfully been applied to various substrates by different techniques to improve their corrosion properties, amongst other metals stainless steel and titanium. (Hernández-Montes, Betancur-Henao, and Santa-Marín 2017).

Considering TiO₂ prepared by ALD for protection of magnesium alloys, the literature available are for now limited. As discussed previously, (Marin et al. 2012) successfully deposited TiO₂ on a AZ31 alloy with the help of ALD who enhanced the corrosion protection. This gives an indication that TiO₂ is a potential candidate with interesting possibilities that needs to be further be evaluated by testing.

3.3.3 HfO₂

HfO₂ prepared by ALD is an interesting candidate for CMOS-technology, and the ALD process for preparing this oxide is therefore well known (Niinistö et al. 2005). Although HfO₂ prepared by ALD has not been evaluated corrosion protection of magnesium, this material is an interesting candidate. Hafnium is in the same chemical group as titanium and zirconium. Due to this fact, hafnium is expected to have similar performance in biocompatibility and corrosion resistance, and have shown to have good corrosion properties due to the formation of HfO₂ (Rituerto Sin, Neville, and Emami 2014).

In a study by (Jin et al. 2016) Hf ion implementation was executed on WE43 magnesium alloy to improve its corrosion resistance and biocompatibility, which was tested in SBF. The treated alloy showed great corrosion properties compared to the untreated alloy. By immersion tests a thick layer of corrosion products formed on the surface, with a few small pits allowing fluids reaching the surface. Additionally, the treated alloy showed good cell adhesion and negligible cytotoxicity.

There is hence reason to believe that HfO₂ for biocorrosion protection has a potential.

4 Results

4.1 Summarizing table on coatings prepared by techniques other than ALD

In Table 4.1, results from different polarization tests conducted on samples coated with various techniques are listed to indicate the corrosion properties of different coating techniques.

Table 4.1 Results from polarization tests conducted on coatings prepared by different coating techniques.

<i>Alloy</i>	<i>Coating material</i>	<i>Thickness</i>	<i>Technique</i>	<i>Highest E_{corr} (V_{SCE})</i>	<i>Lowest i_{corr} (A/cm²)</i>	<i>Test solution</i>	<i>Reference</i>
AZ31	HA	6 μm	<i>Bare</i>	-1.39*	7.3×10^{-6}	SBF	(Tang et al. 2013)
			<i>Dip-coating</i>	-0.70*	3.10×10^{-6}		
AZ31	Nb ₂ O ₅	2 μm	<i>Bare</i>	-1.73	1.19×10^{-4}	SBF	(Amaravathy et al. 2014)
			<i>Dip-coating</i>	-1.5	0.53×10^{-4}		
AZ31B	Ca-P/ HA	8 μm	<i>Bare</i>	-1.7**	3.75×10^{-3}	SBF	(Zheng et al. 2018)
			<i>PEO/Dip-coating</i>	-0.2**	1.25×10^{-5}		
AZ31B	Ca-P	3 μm	<i>Bare</i>	-1.7**	3.75×10^{-3}	SBF	(Zheng et al. 2018)
			<i>PEO</i>	-1.25**	6.50×10^{-4}		
ZK60	P	10 μm	<i>Bare</i>	-1.49	1.18×10^{-5}	Hank's solution	(Lin et al. 2014)
			<i>PEO</i>	-1.60	4.16×10^{-7}		
ZK60	Sr-P	20 μm	<i>Bare</i>	-1.49	1.18×10^{-5}	Hank's solution	(Lin et al. 2014)
			<i>PEO</i>	-1.55	1.51×10^{-7}		
Mg-0.79Ca	O, Mg, Si	6.74 μm	<i>Bare</i>	-1.66	1.21×10^{-4}	Hank's solution	(Cui et al. 2017)
			<i>PEO</i>	-1.60	4.02×10^{-6}		
-	Phosphate	-	<i>Bare</i>	-5.55	6.67×10^{-6}	SBF	(Zhang 2015)
			<i>Conversion coating</i>	-1.39	9.14×10^{-7}		
AZ61	MgF ₂	2.5 μm	<i>Bare</i>	-1.57	2.79×10^{-8}	SBF	

			Conversion coating	-1.06	7.00×10^{-10}		(Fintová et al. 2019)
AZ31	MgF ₂	13.6 μm	<i>Bare</i>	-1.54*	2.47×10^{-5}	Hanks's solution	(Jiang et al. 2017)
			<i>Anodizing</i>	-1.36*	8.53×10^{-6}		
AZ31B	Carbon nitride	4.69 μm	<i>Bare</i>	-1.610	1.32×10^{-5}	PBS	(G. Yang et al. 2018)
			<i>CVD</i>	-1.31	4.61×10^{-6}		
AZ91	Parylene C	2 μm	<i>Bare</i>	-1.33	4.03×10^{-4}	Hanks's solution	(Surmeneva et al. 2018)
			<i>CVD</i>	-0.58	6.42×10^{-7}		
AZ31	Parylene C	2 μm	<i>Bare</i>	-1.19	7.41×10^{-4}	Hanks's solution	(Surmeneva et al. 2018)
			<i>CVD</i>	-0.18	7.24×10^{-7}		
WE43	Parylene C	2 μm	<i>Bare</i>	-1.17	7.71×10^{-5}	Hanks's solution	(Surmeneva et al. 2018)
			<i>CVD</i>	-0.59	3.29×10^{-7}		
Mg-0.8Ca-3Zn	ZnO	1.1 μm	<i>Bare</i>	-1.62	2.02×10^{-4}	SBF	(Bakhsheshi-Rad et al. 2017)
			<i>PVD</i>	-1.44	4.23×10^{-6}		
Mg-0.8Ca-3Zn	ZnO/MWCNT	1.1 μm/ 10.2 μm	<i>Bare</i>	-1.62	2.02×10^{-4}	SBF	(Bakhsheshi-Rad et al. 2017)
			<i>PVD/ Dip-coating</i>	-1.27	7.20×10^{-6}		
AM50	TiO	100nm	<i>Bare</i>	-1.41*	-	SBF	(Abdal-Hay et al. 2014)
			<i>PVD</i>	-1.28*	-		
AM50	TiO/PLA	100nm/ 1.8 μm	<i>Bare</i>	-1.41*	-	SBF	(Abdal-Hay et al. 2014)
			<i>PVD/ Dip-coating</i>	-0.834*	-		

*Reference electrode not SCE but Ag/AgCl

** Values obtained by reading of graph in reference by the author of this project

4.2 Summarizing table on coatings prepared by ALD

In Table 4.2, results from polarization tests on magnesium alloys coated by ALD are summarized.

Table 4.2 Results from polarization tests conducted on coatings prepared by ALD

<i>Alloy</i>	<i>Coating material</i>	<i>Thickness</i>	<i>Technique</i>	<i>Highest E_{corr} (V_{SCE})</i>	<i>Lowest i_{corr} (A/cm^2)</i>	<i>Test solution</i>	<i>Reference</i>
AZ31	ZrO ₂	11.7nm	<i>Bare</i>	-1.557	5.12×10^{-4}	0.9% NaCl	(Liu et al. 2018)
			<i>ALD</i>	-1.462	2.78×10^{-7}		
AZ31	PLGA/ ZrO ₂	-/11.7nm	<i>Bare</i>	-1.557	5.12×10^{-4}	0.9% NaCl	(Liu et al. 2018)
			<i>Spin-coating/ALD</i>	-1.452	4.90×10^{-9}		
Mg-Sr	ZrO ₂	38.8nm	<i>Bare</i>	-1.928	3.07×10^{-4}	SBF	(Q. Yang et al. 2017)
			<i>ALD</i>	-1.75	4.88×10^{-6}		
AZ31	TiO ₂	100nm	<i>Bare</i>	1.48*	10^{-4}	0.05M NaCl	(Marin et al. 2012)
			<i>ALD</i>	-1.61	10^{-6}		
AZ31	Al ₂ O ₃	100nm	<i>Bare</i>	1.48*	10^{-4}	0.05M NaCl	(Marin et al. 2012)
			<i>ALD</i>	-1.46	10^{-6}		
AZ31	Al ₂ O ₃ / TiO ₂ /	100nm	<i>Bare</i>	1.48*	10^{-4}	0.05M NaCl	(Marin et al. 2012)
			<i>ALD</i>	-1.58	10^{-8}		
AZ31	Al ₂ O ₃ / TiO ₂ / Al ₂ O ₃ / TiO ₂ /	100nm	<i>Bare</i>	1.48*	10^{-4}	0.05M NaCl	(Marin et al. 2012)
			<i>ALD</i>	-1.57	10^{-8}		
AZ31	MgO and MgSiO ₄ / AZO	-/100nm	<i>Bare</i>	-1.561	3.16×10^{-4}	3.5wt% NaCl	(Y. Li et al. 2017)
			<i>PEO/ALD</i>	-0.550	1.36×10^{-6}		
Mg-Li	LiAl _x O _y	200nm	<i>Bare</i>	-1.46	2×10^{-3}	3.5wt% NaCl	(P. C. Wang et al. 2010)
			<i>ALD</i>	-1.08	10^{-4}		

*Reference electrode not SCE but Ag/AgCl

5 Discussion

5.1 ALD compared to other coating techniques

After reviewing literature on both ALD and other coatings, there are several aspects that indicate that more attention should be paid to ALD for corrosion protection of magnesium alloys in biomedical use.

Comparing the electrochemical potential and current density results from atomic layer deposited coatings against the coatings prepared by other techniques, one can observe that there is no obvious gap in magnitude. Moreover, when comparing the thicknesses needed to achieve these results, nearly all coatings for other techniques have a coating at μm -scale in contrast to ALD-coatings where all coatings are at nm-scale. This indicates that less material is needed with ALD to achieve desired corrosion properties.

For both conversion coatings, anodizing and sol-gel techniques, the thickness is rather hard to control, hence giving a non-uniform surface. As for degradation mechanisms it is desired to have a uniform coating to secure uniform corrosion, thickness control is an important property for the coating technique. PEO, PVD and traditional CVD-methods provide better thickness control, than the last mentioned, but none is comparable to the conformal coatings created by ALD offering thickness control on atom level. It has been suggested by several papers that the surface roughness of a coating influences biocompatibility, but the conclusions are contradicting (Mochizuki, Yahata, and Takai 2016). Hence, it is too early to say if surface roughness either enhances or worsen biocompatibility.

In the sense of biocompatibility, this highly depends on the composition of the coating, and not the technique. However, the choice of technique is important regarding coating composition control. Amongst the coating techniques discussed above are CVD, including ALD, the only methods offering accurate composition control.

The main motivation for applying a coating on magnesium alloys is corrosion protection, and hence it is important for the coating to completely cover the surface to avoid pitting. Avoiding pores are also important to limit hydrogen evolution in regards of cell viability. For conversion coatings both cracks and pores have been reported as discussed previously, which may induce corrosion. Sol-gel coatings tend to crack upon drying and therefore needs to be carefully examined both before, during and after drying. For PVD-films, poor long-term protection has

been observed and therefore a top-coat have often applied to cover pores in the PVD-coating. This also goes for PEO-films, where discharges cause pores, thus a top-coat is very often necessary. In CVD-coatings the film is dense and smooth, in particular ALD where the film is pinhole-free, which makes these techniques excellent corrosion inhibiting methods.

As magnesium is a heat-sensitive material, low processing temperature during film deposition is important to avoid temperature defects such as phase transformations. However, it should be emphasized that impurities in an ALD coating are decreased with increased temperature (Salmi 2015). ALD is not the only coating technique offering deposition at low temperatures but has its advantage in assuring good adhesion even at low temperatures. PVD processing also offers low temperatures, but unfortunately it is often difficult to control the temperature during deposition and to secure good enough adhesion to the substrate.

Although the properties of an ALD coating are superior in comparison to other techniques, it is noteworthy that ALD is time-demanding compared to other techniques.

5.2 ALD for corrosion protection of magnesium

By the articles discussed in section 3, all work show that the corrosion resistance of magnesium alloys can be greatly increased by ALD coatings. The thin, dense, and pinhole free coating created by ALD is excellent considering corrosion. However, for long-term protection the thickness of the coating should be carefully considered due to some nano-gaps found in the thinner coatings in which cause early failure by galvanic corrosion between the coating and substrate. This problem could be minimized by adding a top coat, but this would give less control of the composition and thickness of the coating and complicate the coating process.

It should be emphasized that only one of the articles discussed, (Q. Yang et al. 2017), investigated a combination of alloy and coating that possibly could be an alternative for implants considering biocompatibility. The other articles involve aluminium in either the coating or alloy, which if released in the body potentially can cause muscle fibre damage, decrease osteoblast viability, be a releasing factor for Alzheimer's disease (Witte et al. 2008), hematotoxicity, neurotoxicity and kidney dysfunction (Liu et al. 2018). Hence, there is a huge need for further research on the field.

6 Conclusion and future work

In this specialization project various coating techniques for biocompatible corrosion protection of magnesium alloys have been reviewed and evaluated. The ALD-process have been introduced, and the current status on protective coatings prepared by ALD on magnesium alloys have been investigated.

In conclusion, there is a large potential laying within ALD for corrosion protection of magnesium alloys for biomedical use. The coating-properties obtained by ALD are superior compared to coatings prepared by other coating techniques alone. The ALD process itself offer great composition control in addition to good adhesion, even at low temperatures, which is crucial for magnesium with its low melting point. Furthermore, there are so far little research on the specific field of ALD on magnesium of clinical applications, but the results available are promising.

ZrO₂, TiO₂ and HfO₂ are all coating-materials that already have been prepared by ALD for various applications. They appear as good candidates for coatings on biomedical magnesium alloys in terms of biocompatibility and corrosion resistance.

For a potential master thesis, experiments will be conducted to provide more knowledge on the subject discussed in this report. ZrO₂, TiO₂ and HfO₂ will be prepared on magnesium alloys by ALD to further investigate the properties of such coatings. To evaluate corrosion properties and biocompatibility, electrochemical polarization tests, electrochemical impedance spectroscopy, and immersion tests to measure weight loss and hydrogen evolution, will be conducted.

References

- Abdal-Hay, Abdalla, Montasser Dewidar, Juhyun Lim, and Jae Kyoo Lim. 2014. "Enhanced Biocorrosion Resistance of Surface Modified Magnesium Alloys Using Inorganic/Organic Composite Layer for Biomedical Applications." *Ceramics International* 40 (1 PART B): 2237–47. <https://doi.org/10.1016/j.ceramint.2013.07.142>.
- Abela, Ing Stephen. 2015. "Physical Vapour Deposition on Mg Alloys for Biomedical Applications." *Surface Modification of Magnesium and Its Alloys for Biomedical Applications 2*: 81–100. <https://doi.org/10.1016/B978-1-78242-078-1.00004-9>.
- Agarwal, Sankalp, James Curtin, Brendan Duffy, and Swarna Jaiswal. 2016. "Biodegradable Magnesium Alloys for Orthopaedic Applications: A Review on Corrosion, Biocompatibility and Surface Modifications." *Materials Science and Engineering C* 68: 948–63. <https://doi.org/10.1016/j.msec.2016.06.020>.
- Amaravathy, P., S. Sowndarya, S. Sathyanarayanan, and N. Rajendran. 2014. "Novel Sol Gel Coating of Nb₂O₅ on Magnesium Alloy for Biomedical Applications." *Surface and Coatings Technology* 244: 131–41. <https://doi.org/10.1016/j.surfcoat.2014.01.050>.
- Asri, R. I.M., W. S.W. Harun, M. A. Hassan, S. A.C. Ghani, and Z. Buyong. 2016. "A Review of Hydroxyapatite-Based Coating Techniques: Sol-Gel and Electrochemical Depositions on Biocompatible Metals." *Journal of the Mechanical Behavior of Biomedical Materials* 57: 95–108. <https://doi.org/10.1016/j.jmbbm.2015.11.031>.
- Augello, C, and H Liu. 2015. "Surface Modification of Magnesium by Functional Polymer Coatings for Neural Applications." In *Surface Modification of Magnesium and Its Alloys for Biomedical Applications*, edited by T. S. N. Sankara Narayanan, Il-Song Park, and Min-Ho Lee, Volume II:, 335–53. Elsevier Ltd. https://doi.org/10.1007/10367682_1.
- Bakhsheshi-Rad, H. R., E. Hamzah, George J. Dias, Safaa N. Saud, F. Yaghoubidoust, and Z. Hadisi. 2017. "Fabrication and Characterisation of Novel ZnO/MWCNT Duplex Coating Deposited on Mg Alloy by PVD Coupled with Dip-Coating Techniques." *Journal of Alloys and Compounds* 728: 159–68. <https://doi.org/10.1016/j.jallcom.2017.08.161>.
- Blawert, C, S P Sah, Nico Scharnagl, and M Bobby Kannan. 2015. "Plasma Electrolytic Oxidation/Micro-Arc Oxidation of Magnesium and Its Alloys." In *Surface Modification of Magnesium and Its Alloys for Biomedical Applications*, edited by T. S. N. Sankara Narayanan, Il-Song Park, and Min-Ho Lee, Volume II:, 193–234. Elsevier Ltd. <https://doi.org/https://doi.org/10.1016/B978-1-78242-078-1.00008-6>.

- Carlsson, Jan Otto, and Peter M. Martin. 2010. *Chemical Vapor Deposition. Handbook of Deposition Technologies for Films and Coatings*. Third Edit. Elsevier Ltd. <https://doi.org/10.1016/B978-0-8155-2031-3.00007-7>.
- Chalker, P. R. 2016. "Photochemical Atomic Layer Deposition and Etching." *Surface and Coatings Technology* 291: 258–63. <https://doi.org/10.1016/j.surfcoat.2016.02.046>.
- Chen, Kai, Jianwei Dai, and Xiaobo Zhang. 2015. "Improvement of Corrosion Resistance of Magnesium Alloys for Biomedical Applications." *Corrosion Reviews* 33 (3–4): 101–17. <https://doi.org/10.1515/corrrev-2015-0007>.
- Chen, X.-B, K Chong, T B Abbott, N Birbilis, and M A Easton. 2015. "Biocompatible Strontium-Phosphate and Manganese-Phosphate Conversion Coatings for Magnesium and Its Alloys." In *Surface Modification of Magnesium and Its Alloys for Biomedical Applications*, edited by T. S. N. Sankara Narayanan, Il-Song Park, and Min-Ho Lee, Volume II., 407–32. Elsevier Ltd. <https://doi.org/https://doi.org/10.1016/B978-1-78242-078-1.00015-3>.
- Chen, Yougui, Ben Li Luan, Guang Ling Song, Qi Yang, David M. Kingston, and Farid Bensebaa. 2012. "An Investigation of New Barium Phosphate Chemical Conversion Coating on AZ31 Magnesium Alloy." *Surface and Coatings Technology* 210: 156–65. <https://doi.org/10.1016/j.surfcoat.2012.09.009>.
- Conceição, Thiago F. da, and Nico Scharnagl. 2015. "Fluoride Conversion Coatings for Magnesium and Its Alloys for the Biological Environment." *Surface Modification of Magnesium and Its Alloys for Biomedical Applications* 2: 3–21. <https://doi.org/10.1016/B978-1-78242-078-1.00001-3>.
- Cui, Lan Yue, Rong Chang Zeng, Shao Kang Guan, Wei Chen Qi, Fen Zhang, Shuo Qi Li, and En Hou Han. 2017. "Degradation Mechanism of Micro-Arc Oxidation Coatings on Biodegradable Mg-Ca Alloys: The Influence of Porosity." *Journal of Alloys and Compounds* 695: 2464–76. <https://doi.org/10.1016/j.jallcom.2016.11.146>.
- Dorozhkin, S. V. 2015. *Surface Modification of Magnesium and Its Biodegradable Alloys by Calcium Orthophosphate Coatings to Improve Corrosion Resistance and Biocompatibility. Surface Modification of Magnesium and Its Alloys for Biomedical Applications*. Vol. 2. Elsevier Ltd. <https://doi.org/10.1016/B978-1-78242-078-1.00007-4>.
- Fintová, Stanislava, Juliána Drábiková, Filip Pastorek, Jakub Tkacz, Ivo Kuběna, Libor Trško, Branislav Hadzima, et al. 2019. "Improvement of Electrochemical Corrosion Characteristics of AZ61 Magnesium Alloy with Unconventional Fluoride Conversion Coatings." *Surface and Coatings Technology* 357 (June 2018): 638–50.

- <https://doi.org/10.1016/J.SURFCOAT.2018.10.038>.
- Grael, Octavio, Matthieu Weber, Sébastien Balme, Philippe Miele, and Mikhael Bechelany. 2018. "Atomic Layer Deposition for Biosensing Applications." *Biosensors and Bioelectronics* 122 (July): 147–59. <https://doi.org/10.1016/j.bios.2018.09.038>.
- Hernández-Montes, Vanessa, Claudia Patricia Betancur-Henao, and Juan Felipe Santa-Marín. 2017. "Titanium Dioxide Coatings on Magnesium Alloys for Biomaterials: A Review TT - Recubrimientos de Dioxido de Titanio Sobre Aleaciones de Magnesio Para Biomateriales: Una Revisión." *Dyna* 84 (200): 261–70. <https://doi.org/10.15446/dyna.v84n200.59664>.
- Hiramoto, Sachiko. 2015. *Chemical Solution Deposition of Hydroxyapatite and Octacalcium Phosphate Coatings for Magnesium and Its Alloys to Improve Biocompatibility. Surface Modification of Magnesium and Its Alloys for Biomedical Applications*. Vol. 2. Elsevier Ltd. <https://doi.org/10.1016/B978-1-78242-078-1.00003-7>.
- Jiang, Heng Bo, Guosong Wu, Sang Bae Lee, and Kwang Mahn Kim. 2017. "Achieving Controllable Degradation of a Biomedical Magnesium Alloy by Anodizing in Molten Ammonium Bifluoride." *Surface and Coatings Technology* 313: 282–87. <https://doi.org/10.1016/j.surfcoat.2017.01.090>.
- Jin, Weihong, Guosong Wu, Ang Gao, Hongqing Feng, Xiang Peng, and Paul K. Chu. 2016. "Hafnium-Implanted WE43 Magnesium Alloy for Enhanced Corrosion Protection and Biocompatibility." *Surface and Coatings Technology* 306: 11–15. <https://doi.org/10.1016/j.surfcoat.2016.02.055>.
- Kääriäinen, Tommi, David Cameron, Marja-Leena Kääriäinen, and Arthur Sherman. 2013. "Titanium Dioxide." In *Atomic Layer Deposition - Principles, Characteristics, and Nanotechnology Applications*, 2nd ed., 81–95. John Wiley & Sons, Incorporated. <https://ebookcentral.proquest.com/lib/ntnu/detail.action?docID=1192829>.
- Kannan, M Bobby. 2015. "Biodegradable Polymeric Coatings for Surface Modification of Magnesium-Based Biomaterials." In *Surface Modification of Magnesium and Its Alloys for Biomedical Applications*, edited by T. S. N. Sankara Narayanan, Il-Song Park, and Min-Ho Lee, Volume II., 355–76. Elsevier Ltd. <https://doi.org/https://doi.org/10.1016/B978-1-78242-078-1.00013-X>.
- Knoops, H. C.M., S. E. Potts, A. A. Bol, and W. M.M. Kessels. 2014. *Atomic Layer Deposition. Handbook of Crystal Growth: Thin Films and Epitaxy: Second Edition*. Second Edi. Vol. 3. Elsevier B.V. <https://doi.org/10.1016/B978-0-444-63304-0.00027-5>.
- Li, Jianfang, Xiangyu Zhang, Xiaojing He, Ruiqiang Hang, Xiaobo Huang, and Bin Tang. 2017.

- “Preparation, Biocompatibility and Wear Resistance of Microstructured Zr and ZrO₂ alloyed Layers on 316L Stainless Steel.” *Materials Letters* 203: 24–27.
<https://doi.org/10.1016/j.matlet.2017.05.106>.
- Li, Yang, Hang Li, Qiyang Xiong, Xiaoming Wu, Jia Zhou, Jinzhu Wu, Xiaohong Wu, and Wei Qin. 2017. “Multipurpose Surface Functionalization on AZ31 Magnesium Alloys by Atomic Layer Deposition: Tailoring the Corrosion Resistance and Electrical Performance.” *Nanoscale* 9 (25): 8591–99. <https://doi.org/10.1039/c7nr00127d>.
- Lin, Xiao, Xiaoming Yang, Lili Tan, Mei Li, Xin Wang, Yu Zhang, Ke Yang, Zhuangqi Hu, and Jianhong Qiu. 2014. “In Vitro Degradation and Biocompatibility of a Strontium-Containing Micro-Arc Oxidation Coating on the Biodegradable ZK60 Magnesium Alloy.” *Applied Surface Science* 288: 718–26. <https://doi.org/10.1016/j.apsusc.2013.10.113>.
- Liu, Xiangmei, Qiuyue Yang, Zhaoyang Li, Wei Yuan, Yufeng Zheng, Zhenduo Cui, Xianjin Yang, Kelvin W.K. Yeung, and Shuilin Wu. 2018. “A Combined Coating Strategy Based on Atomic Layer Deposition for Enhancement of Corrosion Resistance of AZ31 Magnesium Alloy.” *Applied Surface Science* 434: 1101–11. <https://doi.org/10.1016/j.apsusc.2017.11.032>.
- Marin, E., A. Lanzutti, L. Guzman, and L. Fedrizzi. 2012. “Chemical and Electrochemical Characterization of TiO₂/Al₂O₃ atomic Layer Depositions on AZ-31 Magnesium Alloy.” *Journal of Coatings Technology and Research* 9 (3): 347–55. <https://doi.org/10.1007/s11998-011-9372-8>.
- Markowska-Szczupak, A., K. Ulfig, and A. W. Morawski. 2011. “The Application of Titanium Dioxide for Deactivation of Bioparticulates: An Overview.” *Catalysis Today* 169 (1): 249–57. <https://doi.org/10.1016/j.cattod.2010.11.055>.
- Matias, Telma Blanco, Gabriel Hitoshi Asato, Bruno Torquato Ramasco, Walter José Botta, Claudio Shyinti Kiminami, and Claudemiro Bolfarini. 2014. “Processing and Characterization of Amorphous Magnesium Based Alloy for Application in Biomedical Implants.” *Journal of Materials Research and Technology* 3 (3): 203–9. <https://doi.org/10.1016/j.jmrt.2014.03.007>.
- Mochizuki, Akira, Chie Yahata, and Hung Takai. 2016. “Cytocompatibility of Magnesium and AZ31 Alloy with Three Types of Cell Lines Using a Direct in Vitro Method.” *Journal of Materials Science: Materials in Medicine* 27 (9). <https://doi.org/10.1007/s10856-016-5762-x>.
- Moravej, Maryam, and Diego Mantovani. 2011. “Biodegradable Metals for Cardiovascular Stent Application: Interests and New Opportunities.” *International Journal of Molecular Sciences* 12 (7): 4250–70. <https://doi.org/10.3390/ijms12074250>.
- Narayanan, T. S.N.Sankara, Il Song Park, and Min Ho Lee. 2015. *Strategies to Improve the Corrosion*

Resistance of Microarc Oxidation Coatings on Magnesium and Its Alloys: Implications for Biomedical Applications. Surface Modification of Magnesium and Its Alloys for Biomedical Applications. Vol. 2. <https://doi.org/10.1016/B978-1-78242-078-1.00009-8>.

- Niinistö, Jaakko, Matti Putkonen, Lauri Niinistö, Sarah L. Stoll, Kaupo Kukli, Timo Sajavaara, Mikko Ritalac, and Markku Leskeläc. 2005. "Controlled Growth of HfO₂ Thin Films by Atomic Layer Deposition from Cyclopentadienyl-Type Precursor and Water." *Journal of Materials Chemistry*, no. 23. <https://doi.org/10.1039/B417866C>.
- Packham, D E. 2011. *Handbook of Adhesion Technology*. Vol. 1. <https://doi.org/10.1007/978-3-642-01169-6>.
- Peron, Mirco, Jan Torgersen, and Filippo Berto. 2017. "Mg and Its Alloys for Biomedical Applications: Exploring Corrosion and Its Interplay with Mechanical Failure." *MDPI* 234 (5): 1081–84. <https://doi.org/10.3390/met7070252>.
- Piconi, C, and G Maccauro. 1997. "Review: Zirconia as a Ceramic Biomaterial." *Comprehensive Biomaterials* 20: 1–25. <https://doi.org/10.1016/B978-0-08-055294-1.00017-9>.
- Pilliar, R. M. 2015. "Sol-Gel Surface Modification of Biomaterials." In *Surface Coating and Modification of Metallic Biomaterials*, edited by Cuie Wen, 185–217. Elsevier Ltd. <https://doi.org/10.1016/B978-1-78242-303-4.00006-5>.
- Provine, J, Peter Schindler, Jan Torgersen, Hyo Jin Kim, Hans-Peter Karnthaler, and Fritz B. Prinz. 2016. "Atomic Layer Deposition by Reaction of Molecular Oxygen with Tetrakisdimethylamido-Metal Precursors." *Journal of Vacuum Science & Technology A: Vacuum, Surfaces, and Films* 34 (1): 01A138. <https://doi.org/10.1116/1.4937991>.
- Puurunen, Riikka L. 2014. "A Short History of Atomic Layer Deposition: Tuomo Suntola's Atomic Layer Epitaxy." *Chemical Vapor Deposition* 20 (10-11–12): 332–44. <https://doi.org/10.1002/cvde.201402012>.
- Rituerto Sin, J., A. Neville, and N. Emami. 2014. "Corrosion and Tribocorrosion of Hafnium in Simulated Body Fluids." *Journal of Biomedical Materials Research - Part B Applied Biomaterials* 102 (6): 1157–64. <https://doi.org/10.1002/jbm.b.33097>.
- Salmi, Emma. 2015. *Atomic Layer Deposited Coatings for Corrosion Protection of Metals*. Thesis. <https://doi.org/10.1126/science.1254051>.
- Sankara Narayanan, T. S.N., Il Song Park, and Min Ho Lee. 2013. "Strategies to Improve the Corrosion Resistance of Microarc Oxidation (MAO) Coated Magnesium Alloys for Degradable Implants: Prospects and Challenges." *Progress in Materials Science* 60 (1): 1–71. <https://doi.org/10.1016/j.pmatsci.2013.08.002>.

- Sollazzo, Vincenzo, Furio Pezzetti, Antonio Scarano, Adriano Piattelli, Carlo Alberto Bignozzi, Leo Massari, Giorgio Brunelli, and Francesco Carinci. 2008. "Zirconium Oxide Coating Improves Implant Osseointegration in Vivo." *Dental Materials* 24 (3): 357–61.
<https://doi.org/10.1016/j.dental.2007.06.003>.
- Song, Guangling. 2007. "Control of Biodegradation of Biocompatible Magnesium Alloys." *Corrosion Science* 49 (4): 1696–1701. <https://doi.org/10.1016/J.CORSCI.2007.01.001>.
- Staiger, Mark P., Alexis M. Pietak, Jerawala Huadmai, and George Dias. 2006. "Magnesium and Its Alloys as Orthopedic Biomaterials: A Review." *Biomaterials* 27 (9): 1728–34.
<https://doi.org/10.1016/j.biomaterials.2005.10.003>.
- Surmeneva, M. A., A. Vladescu, C. M. Cotrut, A. I. Tyurin, T. S. Pirozhkova, I. A. Shuvarin, B. Elkin, C. Oehr, and R. A. Surmenev. 2018. "Effect of Parylene C Coating on the Antibiocorrosive and Mechanical Properties of Different Magnesium Alloys." *Applied Surface Science* 427: 617–27.
<https://doi.org/10.1016/j.apsusc.2017.08.066>.
- Tang, H, T Z Xin, Y Luo, and F P Wang. 2013. "In Vitro Degradation of AZ31 Magnesium Alloy Coated with Hydroxyapatite by Sol–gel Method." *Materials Science and Technology* 29 (5): 547–52. <https://doi.org/10.1179/1743284712Y.0000000180>.
- Wang, P. C., Y. T. Shih, M. C. Lin, H. C. Lin, M. J. Chen, and K. M. Lin. 2010. "A Study of Atomic Layer Deposited LiAlxOyfilms on Mg-Li Alloys." *Thin Solid Films* 518 (24): 7501–4.
<https://doi.org/10.1016/j.tsf.2010.05.033>.
- Wang, Q., and M. Zhang. 2015. *Cold-Spray Coatings on Magnesium and Its Alloys. Surface Modification of Magnesium and Its Alloys for Biomedical Applications*. Vol. 2. Elsevier Ltd.
<https://doi.org/10.1016/B978-1-78242-078-1.00014-1>.
- Witte, Frank, Norbert Hort, Carla Vogt, Smadar Cohen, Karl Ulrich Kainer, Regine Willumeit, and Frank Feyerabend. 2008. "Degradable Biomaterials Based on Magnesium Corrosion." *Current Opinion in Solid State and Materials Science* 12 (5–6): 63–72.
<https://doi.org/10.1016/j.cossms.2009.04.001>.
- Yang, Guoqiang, Taijun Chen, Bo Feng, Jie Weng, Ke Duan, Jianxin Wang, and Xiaobo Lu. 2018. "Improved Corrosion Resistance and Biocompatibility of Biodegradable Magnesium Alloy by Coating Graphite Carbon Nitride (g-C3N4)." *Journal of Alloys and Compounds* 770: 823–30.
<https://doi.org/10.1016/j.jallcom.2018.08.180>.
- Yang, Qiuyue, Wei Yuan, Xiangmei Liu, Yufeng Zheng, Zhenduo Cui, Xianjin Yang, Haobo Pan, and Shuilin Wu. 2017. "Atomic Layer Deposited ZrO2nanofilm on Mg-Sr Alloy for Enhanced Corrosion Resistance and Biocompatibility." *Acta Biomaterialia* 58: 515–26.

<https://doi.org/10.1016/j.actbio.2017.06.015>.

Zhang, E. 2015. "Phosphate Treatment of Magnesium Alloy Implants for Biomedical Applications." In *Surface Modification of Magnesium and Its Alloys for Biomedical Applications*, edited by T. S. N. Sankara Narayanan, Il-Song Park, and Min-Ho Lee, Volume II:, 23–57. Elsevier Ltd. <https://doi.org/10.1016/B978-1-78242-078-1.00002-5>.

Zheng, Xinhua, Qi Liu, Huijuan Ma, Subhabrata Das, Yanhong Gu, and Lei Zhang. 2018. "Probing Local Corrosion Performance of Sol-Gel/MAO Composite Coating on Mg Alloy." *Surface and Coatings Technology* 347 (January): 286–96. <https://doi.org/10.1016/j.surfcoat.2018.05.010>.

B Potentiodynamic polarisation curves

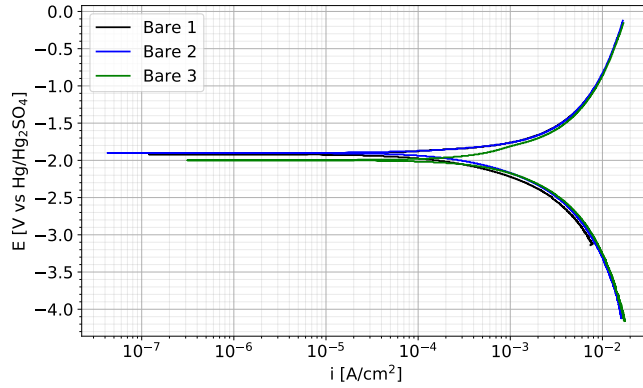


Figure B.1: The potentiodynamic polarisation curves for the bare samples. Note that the first sample was conducted with an electrode potential from -1 to 1 V relative to the OCP.

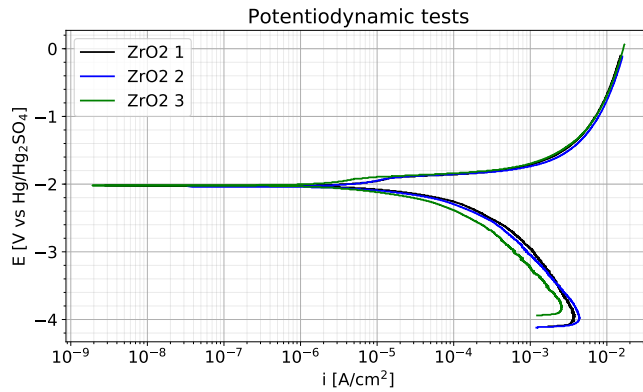


Figure B.2: The potentiodynamic polarisation curves for the ZrO₂-coated samples.

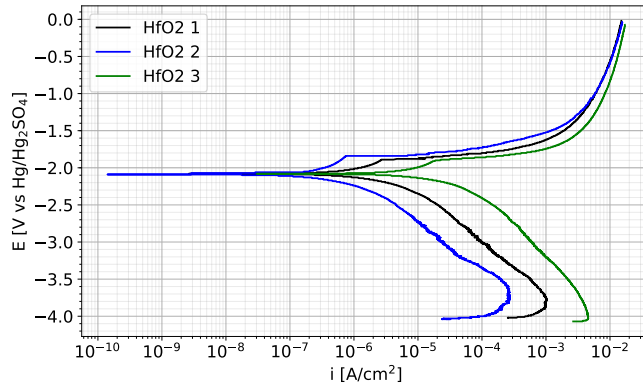


Figure B.3: The potentiodynamic polarisation curves for the HfO_2 -coated samples.

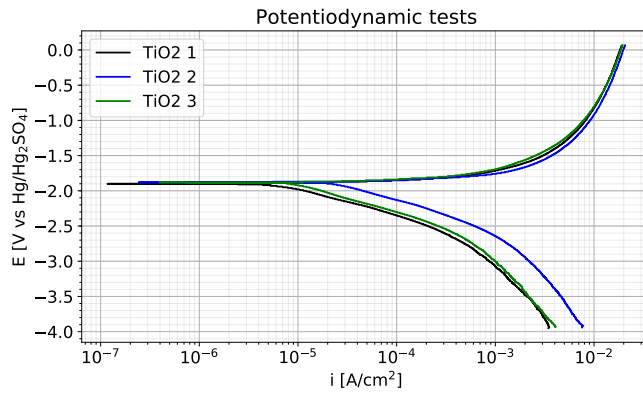


Figure B.4: The potentiodynamic polarisation curves for the TiO_2 -coated samples.

C Risk assessment

NTNU	Hazardous activity identification process			Prepared by	Number	Date
				HSE section	HMSRV2601E	09.01.2013
		Approved by		Replaces		
		The Rector		01.12.2006		



Unit: Department of Mechanical and Industrial Engineering

Date: 30/1-19

Line manager: Torgeir Welø

Participants in the identification process (including their function): J. Torgersen (supervisor), M. Peron (co-supervisor) and Maria Bjelland (student)
Short description of the main activity/main process: Master project for Maria Bjelland. Surface coatings prepared by atomic layer deposition to improve the biocorrosion resistance of magnesium alloys

Is the project work purely theoretical? (YES/NO): NO

Signatures: Responsible supervisor: *Jon Torgersen*

Student:

ID nr.	Activity/process	Responsible person	Existing documentation	Existing safety measures	Laws, regulations etc.	Comment
1	Metallurgical lab	M.B	Room card	First aid kit, eye shower, protective gear, handbook		
1a	Usage of grinding and polishing machines	M.B	Machine's user manual	Safety googles and plastic gloves		
1b	Usage of chemicals	M.B	Data sheet	Safety googles and plastic gloves		
2	Corrosion lab	M.B	Room card	First aid kit, eye shower, protective gear		
2a	Usage of chemicals	M.B	Data sheet	Safety googles and plastic gloves		

NTNU		Risk assessment		Prepared by	Number	Date
				HSE section	HMSRV/2603E	04.02.2011
HSE/IKS				Approved by		Replaces
				The Rector		01.12.2006



Unit: (Department)

Date:

Line manager:

Participants in the identification process (including their function):

Short description of the main activity/main process: Master project for student xx. Project title.

Signatures: Responsible supervisor:

Student:

Activity from the identification process form	Potential undesirable incident/strain	Likelihood (1-5)	Consequence:			Risk Value (human)	Comments/status Suggested measures
			Human (A-E)	Environment (A-E)	Economy/material (A-E)		
1) Metallurgical lab	Fire	2	C	C	D	D	Locate fire hose, extinguisher, fire blanket, emergency exits. Follow the room rules and use room card.
	Incorrect usage resulting in damage of equipment	2	A	B	B	B	Follow the user manual/machine card. Training and planning ahead.
1a) Usage of grinding and polishing machines	Cuts on fingers or hands	3	A	A	A	A	Be alert when using the equipment. Be careful when grinding. Use plastic gloves.
	Loosing the sample/flying object	3	A	A	A	A	Same as above
1b and 2b) Usage of chemicals	Spilling of dangerous chemicals	3	B	A	A	B	Use protective gear, and read the data sheets carefully. Locate eye shower and first aid kit.
2 Corrosion lab	Fire	2	C	C	D	D	Locate fire hose, extinguisher, fire blanket, emergency exits. Follow the room rules and use room card.

NTNU		Risk assessment		Prepared by	Number	Date
 HSE/IKS				HSE section	HMSRV/2603E	04.02.2011
				Approved by The Rector		Replaces 01.12.2006



Likelihood, e.g.:

1. Minimal
2. Low
3. Medium
4. High
5. Very high

Consequence, e.g.:

- A. Safe
- B. Relatively safe
- C. Dangerous
- D. Critical
- E. Very critical

Risk value (each one to be estimated separately):

- Human = Likelihood x Human Consequence
 Environmental = Likelihood x Environmental consequence
 Financial/material = Likelihood x Consequence for Economy/material

Potential undesirable incident/strain

Identify possible incidents and conditions that may lead to situations that pose a hazard to people, the environment and any materiel/equipment involved.

Criteria for the assessment of likelihood and consequence in relation to fieldwork

Each activity is assessed according to a worst-case scenario. Likelihood and consequence are to be assessed separately for each potential undesirable incident. Before starting on the quantification, the participants should agree what they understand by the assessment criteria.

Likelihood

Minimal 1	Low 2	Medium 3	High 4	Very high 5
Once every 50 years or less	Once every 10 years or less	Once a year or less	Once a month or less	Once a week

Consequence

Grading	Human	Environment	Financial/material
E Very critical	May produce fatality/ies	Very prolonged, non-reversible damage	Shutdown of work >1 year.
D Critical	Permanent injury, may produce serious health damage/sickness	Prolonged damage. Long recovery time.	Shutdown of work 0.5-1 year.
C Dangerous	Serious personal injury	Minor damage. Long recovery time	Shutdown of work < 1 month
B Relatively safe	Injury that requires medical treatment	Minor damage. Short recovery time	Shutdown of work < 1week
A Safe	Injury that requires first aid	Insignificant damage. Short recovery time	Shutdown of work < 1day

The unit makes its own decision as to whether opting to fill in or not consequences for economy/material, for example if the unit is going to use particularly valuable equipment. It is up to the individual unit to choose the assessment criteria for this column.


NTNU	Risk assessment			Number	Date
 HSE/IKS				Prepared by HSE section	HMSRV/2603E
		Approved by The Rector		Replaces 01.12.2006	

Risk = Likelihood x Consequence

Please calculate the risk value for "Human", "Environment" and, if chosen, "Economy/materiel", separately.

About the column "Comments/status, suggested preventative and corrective measures":

Measures can impact on both likelihood and consequences. Prioritise measures that can prevent the incident from occurring; in other words, likelihood-reducing measures are to be prioritised above greater emergency preparedness, i.e. consequence-reducing measures.

NTNU		Risk matrix		Number		Date	
				HMSRV2604		8 March 2010	
HSE/KS				Page		Replaces	
				4 of 4		9 February 2010	
				prepared by			
				HSE Section			
				approved by			
				Rector			



MATRIX FOR RISK ASSESSMENTS at NTNU

CONSEQUENCE		E1	E2	E3	E4	E5
		Extremely serious	Extremely serious	Extremely serious	Extremely serious	Extremely serious
D1		D1	D2	D3	D4	D5
		Serious	Serious	Serious	Serious	Serious
C1		C1	C2	C3	C4	C5
		Moderate	Moderate	Moderate	Moderate	Moderate
B1		B1	B2	B3	B4	B5
		Minor	Minor	Minor	Minor	Minor
A1		A1	A2	A3	A4	A5
		Not significant	Not significant	Not significant	Not significant	Not significant
		Very low	Low	Medium	High	Very high
		LIKELIHOOD				

Principle for acceptance criteria. Explanation of the colours used in the risk matrix.

Colour	Description
Red	Unacceptable risk. Measures must be taken to reduce the risk.
Yellow	Assessment range. Measures must be considered.
Green	Acceptable risk. Measures can be considered based on other considerations.